



## PeRL: A Circum-Arctic Permafrost Region Pond and Lake Database

Sina Muster<sup>1</sup>, Kurt Roth<sup>2</sup>, Moritz Langer<sup>3</sup>, Stephan Lange<sup>1</sup>, Fabio Cresto Aleina<sup>4</sup>, Annett Bartsch<sup>5</sup>, Anne Morgenstern<sup>1</sup>, Guido Grosse<sup>1</sup>, Benjamin Jones<sup>6</sup>, A. Britta K. Sannel<sup>7</sup>, Ylva Sjöberg<sup>7</sup>, Frank Günther<sup>1</sup>, Christian Andresen<sup>8</sup>, Alexandra Veremeeva<sup>9</sup>, Prajna R. Lindgren<sup>10</sup>, Frédéric Bouchard<sup>11,13</sup>, Mark J. Lara<sup>12</sup>, Daniel Fortier<sup>13</sup>, Simon Charbonneau<sup>13</sup>, Tarmo A. Virtanen<sup>14</sup>, Gustaf Hugelius<sup>7</sup>, Juri Palmtag<sup>7</sup>, Matthias B. Siewert<sup>7</sup>, William J. Riley<sup>15</sup>, Charles D. Koven<sup>15</sup>, and Julia Boike<sup>1</sup>

10 <sup>1</sup> Alfred Wegener Institute Helmholtz Centre for Polar and Marine Research, Telegrafenberg A43, 14473 Potsdam, Germany

<sup>2</sup> Institute for Environmental Physics, Heidelberg University , Germany

<sup>3</sup> Humboldt University, Berlin, Germany

<sup>4</sup> Max Planck Institute for Meteorology, Hamburg, Germany

<sup>5</sup> Zentralanstalt für Meteorologie und Geodynamik, Vienna , Austria

<sup>6</sup> U.S. Geological Survey - Alaska Science Center, Anchorage, AK 99508, USA

<sup>7</sup> Stockholm University, Department of Physical Geography and the Bolin Centre for Climate Research, 10691 Stockholm, Sweden

<sup>8</sup> Los Alamos National Laboratory, Los Alamos, NM, USA

15 <sup>9</sup> Institute of Physicochemical and Biological Problems in Soil Science, Russian Academy of Sciences, Pushchino, Russia

<sup>10</sup> Geophysical Institute, University of Alaska Fairbanks, Fairbanks, AK, USA

<sup>11</sup> Institut national de la recherche scientifique (INRS), Centre Eau Terre Environnement (ETE), Québec QC, G1K 9A9, Canada

20 <sup>12</sup> Department of Plant Biology, University of Illinois at Urbana-Champaign, Urbana, IL 61801, USA

<sup>13</sup> Geography Department, University of Montréal, Montréal QC, H3C 3J7, Canada

<sup>14</sup> Department of Environmental Sciences, University of Helsinki, Finland

<sup>15</sup> Climate and Ecosystem Sciences Division, Lawrence Berkeley National Laboratory, Berkeley, USA

30 *Correspondence to:* Sina Muster (sina.muster@awi.de)

**Abstract.** Ponds and lakes are abundant in Arctic permafrost lowlands. They play an important role in Arctic wetland ecosystems by regulating carbon, water, and energy fluxes and providing freshwater habitats. However, ponds, i.e. waterbodies with surface areas smaller than  $1.0\text{E+}04 \text{ m}^2$ , have not been inventoried at global and regional scales. The Permafrost Region Pond and Lake Database (PeRL) presents the results of a circum-arctic effort to map ponds and lakes from modern (2002–2013) high-resolution aerial and satellite imagery with a resolution of 5 m or better that resolve waterbodies with a surface area between  $1.0\text{E+}02 \text{ m}^2$  and  $1.0\text{E+}06 \text{ m}^2$ . The database also includes historical imagery from 1948 to 1965 with a resolution of 6 m or better. PeRL includes 69 maps covering a wide range of environmental conditions from tundra to boreal regions and from continuous to discontinuous permafrost zones. Waterbody maps are linked to regional permafrost landscape maps which provide information on permafrost extent, ground ice volume, geology and lithology. This paper describes waterbody classification and accuracy, and presents statistics of waterbody distribution for each site. Maps of permafrost landscapes in Alaska, Canada and Russia are used to extrapolate waterbody statistics from the site level to regional landscape units. PeRL presents pond and lake estimates for a total area of  $1.4\text{E+}06 \text{ km}^2$  across the Arctic, about 17 % of the Arctic lowland (<300 m a.s.l.) land surface area. PeRL waterbodies with



sizes of  $1.0E+06\text{ m}^2$  down to  $1.0E+02\text{ m}^2$  contributed up to 21% to the total water fraction. Waterbody density ranged from  $1.0E+00\text{ per km}^2$  to  $9.4E+01\text{ per km}^2$ . Ponds are the dominant waterbody type by number in all landscapes with 45 % to 99 % of the total waterbody number. The implementation of PeRL size distributions into land surface models will greatly improve the investigation and projection of surface inundation and carbon fluxes in permafrost lowlands. Waterbody maps, study area boundaries and maps of regional permafrost landscapes including link to detailed metadata are available at <https://doi.pangaea.de/10.1594/PANGAEA.868349>.

10 **1 Introduction**

Globally, Arctic lowlands underlain by permafrost have both the highest number and area fraction of waterbodies (Lehner and Döll, 2004; Verpoorter et al., 2014; Grosse et al., 2013). They play key roles as a freshwater resource, as habitat for wildlife, and as part of the water, carbon, and energy cycles (Rautio et al., 2011; Barry et al., 2013).

15 The rapid warming of the Arctic affects the distribution of surface and subsurface water due to permafrost degradation and increased evapotranspiration (Hinzman et al., 2013). Remote sensing studies have found both increasing and decreasing trends in surface water extent for lakes in permafrost regions across broad spatial and temporal scales (Smith et al., 2005; Riordan et al.; 2006; Carroll et al., 2011; Watts et al., 2012; Boike et al. 2016; Kravtsova and Rodionova, 2016). These studies, however, are limited in their assessment of changes in 20 surface inundation since they only include lakes, *i.e.*, waterbodies with a surface area of  $1.0E+04\text{ m}^2$  or larger. Ponds with a surface area smaller than  $1.0E+04\text{ m}^2$ , on the other hand, have not yet been inventoried on the global scale. Yet ponds dominate the total number of waterbodies in Arctic lowlands, accounting for up to 95% of individual waterbodies, and may contribute up to 30% of the total water surface area (Muster et al., 2012, 2013). Arctic ponds are characterized by intense biogeophysical and biogeochemical processes. They have been 25 identified as a large source of carbon fluxes compared to the surrounding terrestrial environment (Rautio et al., 2011; Laurion et al., 2010; Abnizova et al., 2012; Langer et al., 2015; Bouchard et al., 2015; Wik et al., 2016). Due to their small surface areas and shallow depths, ponds are especially prone to change; various studies reported ponds to dry out or to increase in abundance due to new thermokarst or drainage of large lakes (Jones et al., 2011; Andresen and Lougheed et al., 2015; Liljedahl et al., 2016). Such changes in surface 30 inundation may significantly alter regional water, energy, and carbon fluxes (Watts et al., 2014; Lara et al., 2015). Both monitoring and modeling of pond and lake development are therefore crucial to better understand the trajectories of Arctic land cover dynamics in relation to climate and environmental change. Currently, however, the direction and magnitude of these changes remain uncertain, mainly due to the limited extent of high-resolution studies and the lack of pond representation in global databases. Although recent efforts have 35 produced global land cover maps with resolutions of 30 m (Verpoorter et al., 2014; Liao et al., 2014; Feng et al., 2015; Paltan et al., 2015), these data sets only include lakes.

To complement previous approaches, we present the Permafrost Region Pond and Lake Database (PeRL), a circum-arctic effort to map ponds and lakes from remote sensing data with high spatial resolution (of  $\leq 6\text{ m}$ ). This database fills the gap in available global databases that have cutoffs in waterbody surface area at  $1.0E+04\text{ m}^2$  or above. In addition, we link PeRL waterbody maps with existing maps of permafrost landscapes to 40



extrapolate waterbody distributions from the individual study areas to larger landscapes units. Permafrost landscapes are terrain units characterized by distinct properties such as climate, surficial geology, parent material, permafrost extent, ground ice content, and topography. These properties have been identified as major factors in the evolution and distribution of northern waterbodies (Smith et al., 2007; Grosse et al., 2013;

5 Veremeeva and Glushkova, 2016).

The core objectives of the PeRL database are to (i) archive and disseminate fine-resolution geospatial data of northern high latitude waterbodies ( $\leq 6$  m spatial resolution), (ii) quantify the intra- and interregional variability in waterbody size distributions, and (iii) provide regional key statistics, including the uncertainty in waterbody distributions, that can be used to benchmark site-, regional-, and global-scale land models.

10

## 2 Definition of ponds and lakes

The definition of ponds and lakes varies in the literature and depends on the chosen scale and goal of studies when characterizing waterbodies. The Ramsar classification scheme defines ponds as permanently inundated basins smaller than  $8.0E+04$  m<sup>2</sup> in surface area (Ramsar Convention Secretariat, 2010). Studies have also used

15 surface areas smaller than  $5.0E+04$  m<sup>2</sup> (Labrecque et al. 2009) or  $1.0E+04$  m<sup>2</sup> (Rautio et al., 2011) to distinguish ponds from lakes.

In remote sensing studies, surface area is the most reliably inferred parameter related to waterbody properties. Physical and biogeochemical processes of waterbodies, however, also depend strongly on waterbody depth. Differences in thermodynamics are associated with water depth, where deeper lakes may develop a stratified

20 water column while shallow ponds remain well mixed. In high latitudes, waterbodies with depths greater than 2 m are likely to remain unfrozen at the bottom throughout winter, with implications for overwintering habitat availability for fish and other aquatic species. In permafrost regions, a continuously unfrozen layer (talik) may develop underneath such deeper ponds, which strongly affects carbon cycling in these sediments (Schuur et al.,

2008). Several studies have shown a positive correlation between waterbody surface area and depth (Langer et al., 2015; Wik et al., 2016). However, there is large variability in the area-depth relationship, i.e., there are shallow lakes that freeze to the bottom and ponds that develop a talik, and these characteristics may also change

25 over time with changes in water level and basins morphology. In this study we distinguish ponds and lakes based on their surface area. We adopt the distinction of Rautio et al. (2011) and define ponds as bodies of largely standing water with surface area smaller than  $1.0E+04$  m<sup>2</sup> and lakes as waterbodies with surface area of

30  $1.0E+04$  m<sup>2</sup> or larger.

## 3 Study areas

PeRL study areas are widely distributed throughout Arctic lowlands in Alaska, Canada, Europe, and Russia and cover a latitudinal geographic gradient of 20° (55.3°N to 75.7°N), including tundra to boreal regions, continuous

35 to discontinuous permafrost zones (Fig. 1). Mean annual temperature ranges from 0 °C to -20 °C and average annual precipitation ranges from 97 mm to 650 mm (Table 1).

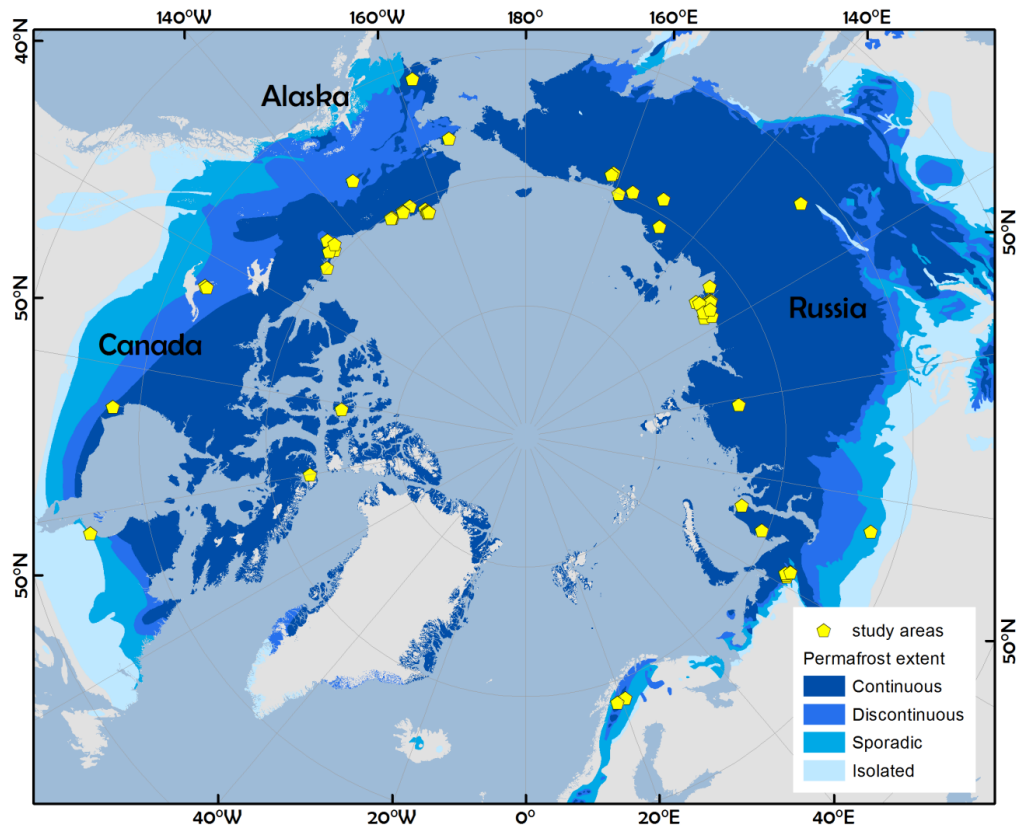


Fig. 1: Distribution of PeRL study areas. Permafrost extent according to Brown et al. (1998).



Table 1: Climate and permafrost characteristics for each study area. Mean annual air temperature (MAAT), total precipitation (TP), permafrost extent (PE, C-continuous, D-discontinuous, S-sporadic, I-isolated), permafrost depth (PT). References to all data sources are listed in the supplement (Table A1).

country	map ID	site name	lat	long	MAAT [°C]	TP [mm]	PE	PT [m]
Alaska	yfl001	Yukon Flats Basin	66.2	-145.9	-5	309	D	90
Alaska	ksl001	Kotzebue Sound Lowlands	66.2	-165.8	-3	427	C	<50
Alaska	imc001	Ikpikpuk Middle Coastal Plain	70.2	-153.3	-10	97	C	260
Alaska	fis001	Fish-Judy Creek Floodplain	70.3	-151	-10	97	C	260
Alaska	kcp001, kpc002, kpc003	Kuparuk Coastal Plain	70.3	-148.5	-10	97	C	260
Alaska	bar001, bar002, bar003, bar004	Barrow Peninsula	70.9	-156.2	-11	115	C	>400
Alaska	elc001, elc002, elc003	Elson Lagoon Coast Plain	71.2	-156.4	-11	115	C	>400
Alaska	yuk001, yuk002	Yukon-Kuskokwim Delta		-162	61	471	C	100-200
Canada	gpr001	Grande Rivière de la Baleine Plateau	55.3	-77.5	-4	650	S	10-50
Canada	hbl001	Coastal Hudson Bay Lowlands	57.9	-94.2	-6	430	C	NA
Canada	tbr001, tea001	Tanzin Upland Beaufieu River	62.7	-115.2	-4	289	D	NA
Canada	mdw001	Mackenzie Delta North	68.5	-134.7	-8	241	D	<100-500
Canada	mdn001	Mackenzie Delta West	69.1	-135.2	-8	241	D	<100-500
Canada	esk001	Eskimo Lakes	69.2	-133.3	-10	161	C	750
Canada	ric001	Richards Island	69.5	-134.3	-8	241	C	>400
Canada	tuk001	Tuktoyaktuk Peninsula	69.9	-130.4	-10	161	C	750
Canada	byl001	Bylot Island	73.2	-80.0	-15	190	C	>200
Canada	pbp001	Polar Bear Pass	75.7	-98.5	-16	161	C	>500
Russia	yak001	Yakutsk	62.1	130.3	-10	228	C	200-300
Russia	rog001, rog003, rog004, rog005	rog002, Rogovaya	62.3	62.1	-6	538	C	ca. 50
Russia	sur001	Surgut	62.3	74.6	-17	400	S	50-300
Russia	sei001, sei002	Seida	67.1	62.9	-6	470	C	ca. 50
Russia	che001, che002	Cherskii	68.8	161.6	-12	294	C	400-500
Russia	kol002	Kolyma Lowlands	69.5	156.3	-13	144	C	500-600



country	map ID	site name	lat	long	MAAT [°C]	TP [mm]	PE	PT [m]
Russia	ind001, kyt001	Indigirka Lowlands, Kytalik	69.7	148.8	-14	232	C	>300
Russia	kol001	Kolyma Lowlands	70.0	159.1	-10	110	C	500-600
Russia	yam001, yam002	Yamal Peninsula	71.5	70.0	-6	260-400	C	100-500
Russia	byk001	Bykovsky Peninsula	71.8	129.3	-13	427	C	500-600
Russia	sam001	Samoylov Island	72.4	126.5	-13	124	C	400-600
Russia	ice003	Ice complex, Lena Delta	72.8	124.7	-13	124	C	400-600
Russia	fir001, fir002, fir003	First Terrace, Lena Delta	72.9	127.3	-13	124	C	400-600
Russia	ole001	Olenek channel, Lena Delta	72.9	122.9	-15	206	C	200-600
Russia	kur001, kur002	Kurungmakh, Lena Delta	73.2	125.1	-13	124	C	400-600
Russia	log001	Logata	73.4	98.5	-13	270	C	NA
Russia	arg001, arg002	Arga Island	73.5	123.6	-13	124	C	400-600
Sweden	abi001	Abisko	68.3	19.1	0	362	S	>16
Sweden	tav001	Tavvavuoma	68.5	20.9	-3	451	C	<25



## 4 PeRL Database Generation

### 4.1 Data sources and processing

PeRL compiles both previously published and unpublished fine-scale waterbody maps. All waterbody maps were derived from optical or radar airborne or satellite imagery with spatial resolutions of  $\leq 6\text{m}$  that were acquired between mid and late summer (July–September), thereby excluding the snow melt and early summer season. Modern imagery dates from 2002–2013 and historical imagery dates from 1948–1965. Historical imagery allows high-resolution change detection of ponds and lakes.

Previously published maps were originally created for a variety of purposes and from various experts which leads to a broad range of image types and classification methods used. For details on image processing and classification procedures for already published maps ( $n=31$ ) we refer to the supplement (Table B1 and B2) and the respective publications. Twenty-eight maps were specifically produced for PeRL for which we provide the methods in the following section 4.2. Sections 4.3 to 4.6 then describe methods applicable to all waterbody maps.

### 4.2 PeRL image processing and classification

#### 4.2.1 TerraSAR-X imagery

TerraSAR-X imagery was available for sites in the Mackenzie Delta, Tuktoyaktuk Coastlands, and Tazan Uplands in Canada; the Beaufort Coastal Plain and the Yukon Delta in Alaska; and the West Siberian Lowlands and Yamal Peninsula in Russia. TerraSAR-X imagery was acquired in Stripmap Mode with an HH polarization as the geocoded Enhanced Ellipsoid Corrected (EEC) product or as the Single Look Slant Range Complex (SSC) product which was then processed to EEC. Geocoded EEC products obtained from DLR are delivered in radar brightness. They are projected to the best available DEM, *i.e.*, SRTM X band DEMs (30 m resolution) and SRTM C band DEMs (90 m resolution). For the remaining areas, the 1 km resolution GLOBE30 DEM is used. The EEC is a detected multi-look product with reduced speckle and approximately square cells on ground. The slant-range resolution of the image is 1.2 m, which corresponds to 3.3–3.5 m projected on the ground for incidence angles between 45° and 20° and an azimuth resolution of 3.3 m (Eineder et al., 2008). SSC were geocoded to the DUE Permafrost DEM (Santoro and Cartus, 2010) and no multi-looking was applied. TSX data were despeckled in ENVI 4.7 using a lee filter with a 3x3 pixel window followed by a gamma filter with a 7x7 or 11x11 window depending on the image quality (Klonus et al., 2008).

#### 4.2.2 Optical imagery

Optical imagery used for PeRL map production included aerial imagery, GeoEye, QuickBird, WorldView-1 and -2, and KOMPSAT-2 imagery. Pixel resolutions ranged from less than 1 m to 4 m. Most imagery provided a near-infrared band that was used for classification with the exception of WorldView 1 that only has a panchromatic band. Preprocessing of the imagery involved georeferencing or orthorectification depending on availability of high resolution digital elevation models (Table B2).



#### 4.2.3 Classification of open water

Both TerraSAR-X and optical imagery were classified using either a density slice or an unsupervised k-means classification in ENVI v4.8 (ITTVIS). The panchromatic, the near-infrared and the X-Band (HH-polarization) show a sharp contrast between open water and surrounding vegetation. Visual inspection of the imagery could therefore be used to determine individual thresholds values (in case of density slice) or to assign classes (in case of k-means unsupervised classification) for extraction of water surfaces. Threshold values and class boundaries varied between images and sites due to different illumination and acquisition geometry and different sensor spectroradiometry. Detailed information on remote sensing imagery and classification procedure for each site is listed in the supplement (Table B1 and B2).

#### 10 4.3 Post-processing of waterbody maps

Classification results from raster image processing were converted to ESRI vector files in ENVI v4.8 (ITTVIS) so that each waterbody is represented as a single polygon. Commission errors occurred where high reflectance from lake bottoms, turbid waters, shadows or waves on the water surface resulted in higher digital number (DN) values and therefore a misclassification of water as land. Many of these commission errors result in gaps or holes in the lake surface which were removed with a gap-filling procedure in ArcGIS. Partial lakes within the study area were edited manually. Partial lakes along the study area boundaries, segments of streams and rivers, and shadows due to clouds or topography were removed. Minimum waterbody size was set to at least 4 pixels and all classified objects smaller than the minimum size were removed.

Three study areas in the Hudson Bay Lowlands (Canada), Lapland (Sweden), and the Usa River basin (Russia), 20 feature multi-temporal but very small waterbody maps with extents less than 4 km<sup>2</sup> and less than 300 waterbodies. They also contain partial waterbodies along the study area boundaries. Partial lakes were not removed in order to retain the maximum information about waterbody boundaries for change detection analysis. Very large waterbody maps in the Lena Delta and Yakutsk region include river and stream segments that were not manually corrected. Compared to manually refined classifications in the same area, these RapidEye classifications showed a higher 25 estimation of pond number by 35% and of pond surface area by 21%. Information about whether a map includes partial lakes or misclassification areas is given in the metadata (Table B1).

#### 4.4 Study area boundaries

Each waterbody map is associated with a vector file that delineates the study area's boundary. Boundaries were calculated for each map in ArcGIS 10.2 by first producing a positive buffer of 1km to 3 km around each waterbody 30 in the map and merging the individual buffers into one single polygon. From that single buffer we then subtracted again the same distance which rendered the study area boundary. The area of the boundary is referred to as the total mapped area of that site. For sites with multi-temporal data, the total mapped area of the oldest classification was chosen as a reference in order to calculate changes in pond and lake statistics over time.



#### 4.5 Accuracy assessment of classifications

Three study areas in the Hudson Bay Lowlands (Canada), Lapland (Sweden), and the Usa River basin (Russia), feature multi-temporal but very small waterbody maps with extents less than 4 km<sup>2</sup> and less than 300 waterbodies. They also contain partial waterbodies along the study area boundaries. Partial lakes were not removed in order to 5 retain the maximum information about waterbody boundaries for change detection analysis. Very large waterbody maps in the Lena Delta and Yakutsk region include river and stream segments that were not manually corrected. Compared to manually refined classifications in the same area, these RapidEye classifications showed a higher estimation of pond number by 35% and of pond surface area by 21%. Information about whether a map includes partial lakes or misclassification areas is given in the metadata (Table B1).

10    **4.6 PeRL statistical analysis**

Statistics were calculated for all waterbodies, as well as separately for ponds and lakes. We calculated areal fraction, i.e., the area fraction of water relative to land (the total mapped area), number of individual water bodies per km<sup>2</sup>, and mean, median, and standard deviation of surface area for each site using the software package R version 3.3.1. The representativity of these parameters is subject to the study area size, its location within a 15 landscape, and the image resolution. Image resolution defines the minimum object size that can be confidently mapped, whereas study area size determines if very large lakes can be representatively captured. For statistical comparison, we therefore included only waterbodies with sizes of 1.0E+06 down to 1.0E+02 m<sup>2</sup>. Additionally, imagery may capture a certain variation of the landscape's waterbody distribution which may not be representative of the larger landscape. In order to determine a representative total mapping area we compared the variability of 20 probability density functions (PDF) and distribution parameters within three study areas in Russia, Canada, and Alaska. In each study area, we performed a subgrid analysis, i.e., we selected waterbodies from a minimum of 5 and up to 50 randomly distributed boxes with varying sizes of 5x5 km, 10x10 km, and 20x20 km. We calculated the standard error of the mean of all statistical parameters across all boxes of the same size. Relative error of density (waterbody number per km<sup>2</sup>) and waterbody mean surface area was lowest for 10x10 km boxes. Relative error 25 increased with 20x20 km boxes which is probably due to the significantly lower number of boxes that can be sampled from the study areas. Only 12 PeRL sites have a study area larger than 1000 km<sup>2</sup> that would allow us to sample a minimum of 5 boxes of 20x20 km in size. A box size of 10x10 km allows the subsampling of 26 sites with a minimum of 5 boxes. Taking into account the overall variability of distributions and the possible number of subgrid samples, a box size of 10x10 km was chosen for subgrid analysis. Subgrid analysis was conducted for study 30 areas larger than 300 km<sup>2</sup> and the mean of each statistical parameter along with the relative error across the 10x10 km subsets is reported.

#### 4.6 Regional maps of pond and lake distributions

Regional maps of permafrost landscapes were used to extrapolate waterbody maps for lowlands with elevations lower than 300 m a.s.l.. We define permafrost landscapes as a unique combination of climate, geology, lithology, 35 permafrost extent and ground ice volume. Vector maps of these landscape properties are available on the regional



level: the Alaskan map of permafrost characteristics (AK2008) (Jorgensen et al., 2008), the National Ecological Framework for Canada (NEF) (Marshall et al., 1999), and the Land Resources of Russia (LRR) (Stolbovoi and McCallum, 2002). Despite differences in mapping approaches and terminology, the databases report similar landscape characteristics at comparable scales. All regional maps were available as vector files which were  
5 converted to a common North Pole Lambert Azimuthal Equal-Area (NPLAEA) projection. All PL maps were clipped in ArcGIS v10.4 with a lowland mask including only areas with elevations of 300 m or lower. The lowland mask was derived for the whole Arctic using the digital elevation model GTOPO30 (USGS). Vector files of permafrost landscapes are available for Alaska, Canada and Russia. Processing of each map is described in detail in the sections 4.6.1, 4.6.2 and 4.6.3. Attributes of all regional and circum-arctic vector files of permafrost landscapes  
10 are described in Tables C1, C2, C3, and C4.

#### 4.6.1 Alaskan permafrost landscape maps

The PL map of Alaska reports surficial geology, MAAT, primary soil texture, permafrost extent, ground ice volume, and primary thermokarst landforms (Jorgensen et al., 2008). A rule-based model was used to incorporate MAAT and surficial geology. Permafrost characteristics were assigned to each surficial deposit under varying temperatures  
15 using terrain-permafrost relationships and expert knowledge (Jorgensen et al., 2008).

#### 4.6.2 Canadian permafrost landscape maps

Permafrost landscapes of Canada are described in the National Ecological Framework (NEF). The NEF distinguishes four levels of generalization nested within each other. Ecozones represent the largest and most generalized units followed by ecoprovinces, ecoregions, and ecodistricts. Ecodistricts were delineated based mainly  
20 on differences in parent material, topography, landform and soil development derived from the Soil Landscapes of Canada (Soil Landscapes of Canada Working Group, 2010) at a map scale of 1:3,000,000 to 1:1,000,000 (Ecological Stratification Working Group, 1995; Marshall, 1999) whereas ecoregions and ecoprovinces are generalized based mainly on climate, physiography, and vegetation. Ecodistricts were therefore chosen as most appropriate to delineate permafrost landscapes. NEF reports the areal fraction of the underlying soil landscape units and attributes nested  
25 within each ecodistrict. The dominant fraction of surficial geology, lithology, permafrost extent and ground ice volume was chosen to describe each ecodistrict. Ecodistricts with the same permafrost landscape type within the same ecozone were then merged to PL units.

#### 4.6.3 Russian permafrost landscape characterization

In Russia, information about permafrost extent, ground ice content, generalized geology and lithology was available  
30 only as individual vector maps. The individual maps were combined in ArcGIS 10.4 to delineate Russian PL units similar to the Canadian and Alaskan databases. Russian ecozones were mapped using the global-scale map by Olson et al. (2001) which conforms to the Alaskan and Canadian ecozones. The geometric union of ecozone, ground ice content, and permafrost extent was calculated in ArcGIS 10.1 via the tool “intersect”. Each unique combination of these three variables was assigned the dominant fraction of geology and lithology type.



#### 4.6.4 Integration of regional permafrost landscapes

The individual regional PL maps were merged in ArcGIS to produce a unified vector file and map representation (*PeRL\_perma\_land.shp*). Landscape attributes that were retained from the original regional maps were ecozone, permafrost extent, ground ice volume, surficial geology, and lithology (soil texture). Variable names were 5 consolidated using uniform variable names (Table 2). Each polygon in the vector file is assigned a unique ID. The first digit stands for the region (1 – Alaska, 2 – Canada, 3 – Russia), digits 2–6 identify the single polygon, and the last three digits identify the ecozone.

Table 2: Terminology for permafrost properties in the regional permafrost databases of Alaska (AK2008),  
10 Canada (NEF), and Russia (LRR).

Description	PeRL	AK2008	NEF	LRR
ecozone	ECOZONE	NA	ecozone	NA
surficial geology	GEN_GEOL	AGGRDEPOS	UNIT	PARROCK
lithology	LITHOLOGY	TEXTURE	TEXTURE	TEXTUR
permafrost extent	PF_EXTENT	PF_EXTENT	PERMAFROST	EXTENT_OF_
ground ice	GROUND_ICE	ICECLOWASS	PERMAFROST	MIN_MAX

#### 4.6.5 Extrapolation of waterbody statistics to permafrost landscapes

Waterbody maps were spatially linked with their associated permafrost landscape. Maps within the same landscape 15 were combined whereas maps spanning two or more landscapes were divided by selecting all waterbodies that intersected with the respective permafrost landscape. Generally, waterbody statistics were extrapolated for study areas with single or combined total mapped areas of 1.0E+02 km<sup>2</sup> or larger. Maps in the Canadian High Arctic were smaller than 1.0E+02 km<sup>2</sup> but represent typical wetlands in that region and were therefore included in the extrapolation. Several maps within one permafrost landscape were combined and average statistics were calculated 20 across all maps in that permafrost landscape unit. If 10 x 10 km subsets could be sampled within one study area or more than four different maps averaged, the relative error was calculated and reported for each statistic. Historical maps and RapidEye classifications affected by large-scale inclusion of rivers and streams (see section 4.5) were not included in the extrapolation.

Extrapolated values were assigned two confidence classes: high (1) and low (2) confidence. Permafrost landscapes 25 were assigned a high confidence if a map was present in the permafrost landscape of that ecozone. If in the same permafrost landscape but in a different ecozone, the same waterbody statistics were assigned with a low confidence. Due to differences in methodology of mapping and extrapolating permafrost and landscape characteristics, the extrapolation was conducted only within each region. Figures D1, D2, D3, and D4 show the location of waterbody maps within their associated permafrost landscape.



## 5 PeRL database features and accuracy

The database provides two different map products: (i) site level waterbody maps and (ii) an extrapolated circum-arctic waterbody map. The database also provides different tables which present statistical parameters for each individual waterbody map and aggregated statistics for PL unit in the circum-arctic map.

### 5.1 Site-level waterbody maps

The database features altogether 69 individual waterbody maps as ESRI shape-files. Each waterbody shape-file is named according to a map ID. The map ID consists of a three letter abbreviation of the site name, followed by a running three-digit number and the acquisition date of the base imagery imagery (YYYY-MM-DD). Vector files were projected to the NPLAEA projection. Area and perimeter of each waterbody and site was calculated in ArcGIS 10.4 in square meters. Each vector file is accompanied by an xml-file which lists metadata about classification and references as presented in Tables B1 and B2. Each map has a polygon associated with it that describes the study area, *i.e.*, the total land area of the waterbody map. All study areas are stored in the file *PeRL\_study\_areas.shp* and can be identified via the map ID. The study area shape-file also includes the site characteristics listed in Table 1. Twenty-one sites are located in Alaska covering an area of 7.3E+03 km<sup>2</sup>. Canada has 14 sites covering 6.4E+03 km<sup>2</sup> 15 and Russia has 30 sites covering 2.9E+03 km<sup>2</sup>. Four sites are located in Sweden with a total mapped area of 41 km<sup>2</sup>. The database includes six multi-temporal classifications in the Kotzebue Sound Lowlands and on the Barrow Peninsula, Alaska (Andresen et al., 2015), on the Grande Rivière de la Baleine Plateau (Bouchard et al., 2014) and Hudson Bay Lowlands in Canada, Lapland in Sweden, and the Usa River basin in Russia (Hugelius et al.; 2011, Sannel and Kuhry, 2011). Ponds contributed about 45 to 99 % of the total number of waterbodies with a mean of 85 20 ± 14 % and up to 34 % to the total water surface area with a mean of 12 ± 8.3 % (Fig. 2 and Table E1, E2, E3, E4). Mean surface area ranged from 7.9E+01 m<sup>2</sup> with a standard deviation (sd) of 1.2E+01 m<sup>2</sup> on Bylot Island, Canada, to 7.1E+04 m<sup>2</sup> ± 1.5E+05 m<sup>2</sup> on Eskimo Islands, Canada (Table E2). Water fraction of the total mapped area ranged from about 1% to 21% for all waterbodies and from >1 % up to 6% for ponds. Waterbody density ranged from 1.0E+00 per km<sup>2</sup> in Indigirka Lowlands (RUS) to 9.4E+01 per km<sup>2</sup> in Olenek Channel, Lena Delta (RUS).

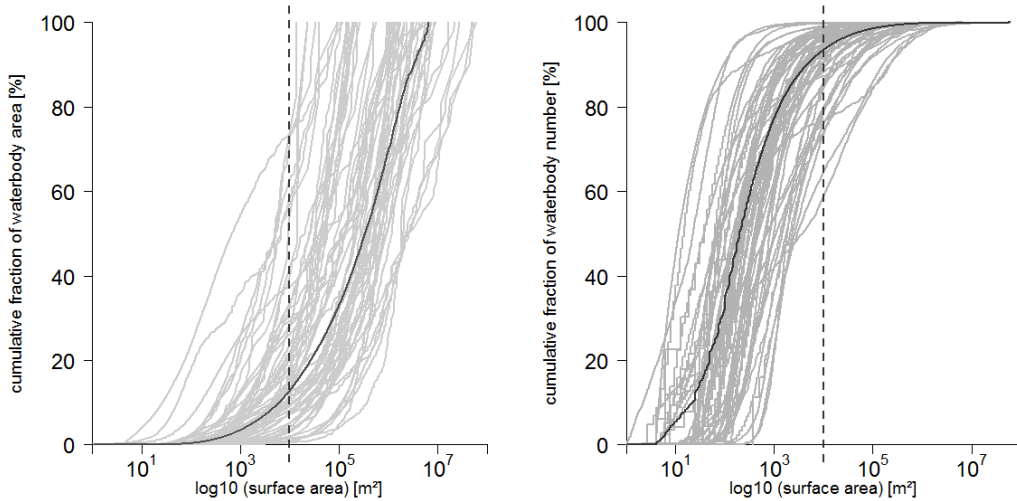


**Fig. 2:** Empirical cumulative distribution function of waterbody area (left hand side) and waterbody number (right hand side). Grey lines represent individual sites across all regions. Black lines represent the mean function averaged over all sites. Vertical dashed line in each panel represents the pond-lake size threshold used in this paper.

## 5 5.2 Circum-arctic waterbody map

Altogether we identified 230 different permafrost landscapes in the Russian lowlands, 160 in the Canadian lowlands, and 51 in the lowlands of Alaska. PeRL waterbody maps were located in 28 different permafrost landscapes (Table 3) covering a total area of  $1.4E+06$  km $^2$  across the Arctic; thereof  $1.0E+06$  km $^2$  in Russia,  $2.1E+05$  km $^2$  in Canada and  $1.7E+05$  km $^2$  in Alaska. About 65% of the extrapolated area was classified as high confidence (Fig. 3).

10 Landscape average areal fraction of water surface reached maxima of 21 % (Fig. 4 and Table 3) and density per km $^2$  of 57 (Fig. 5 and Table 3).

Relative error (RE) for different subsets or maps within a permafrost landscape was about 7 % on average with a maximum of 30 % (Table 2). RE for waterbody density was 8% on average with a maximum of 50 %. Our extrapolated area ( $1.4E+06$  km $^2$ ) represented 17.0 % of the current Arctic permafrost lowland area (below 300 m a.s.l. elevation). PeRL provided pond and lakes estimates for about 29 % (in area) of the Alaskan lowlands, 7 % of the Canadian lowlands, and 21 % of the Russian lowlands. Together all extrapolated landscapes contributed about 7% to the current estimated Arctic permafrost area (Brown et al., 1998). In Alaska, waterbody maps were missing for permafrost landscapes with isolated permafrost (16% of total area) or rocky lithology (36% of total area). Dominant types of surficial geology that were not mapped include colluvial sites, and sites with bedrock or of glacial origin

15 which together contribute 61% to the total area. In Canada, both isolated and sporadic permafrost were not inventoried (22% of total area), as well as areas with ground ice content of 10-20 % or less (23% of total area). Six

20



of the 19 geology classes were inventoried which contribute 75% to the total area. Six of seven lithology types with an areal coverage of 90 % were represented. In Russia, waterbody maps were not available in the discontinuous permafrost zone (13 % of the total area). No maps were present in regions with the geological type “deluvial-coluvial and creep” which accounts for 28 % of the total area.

5

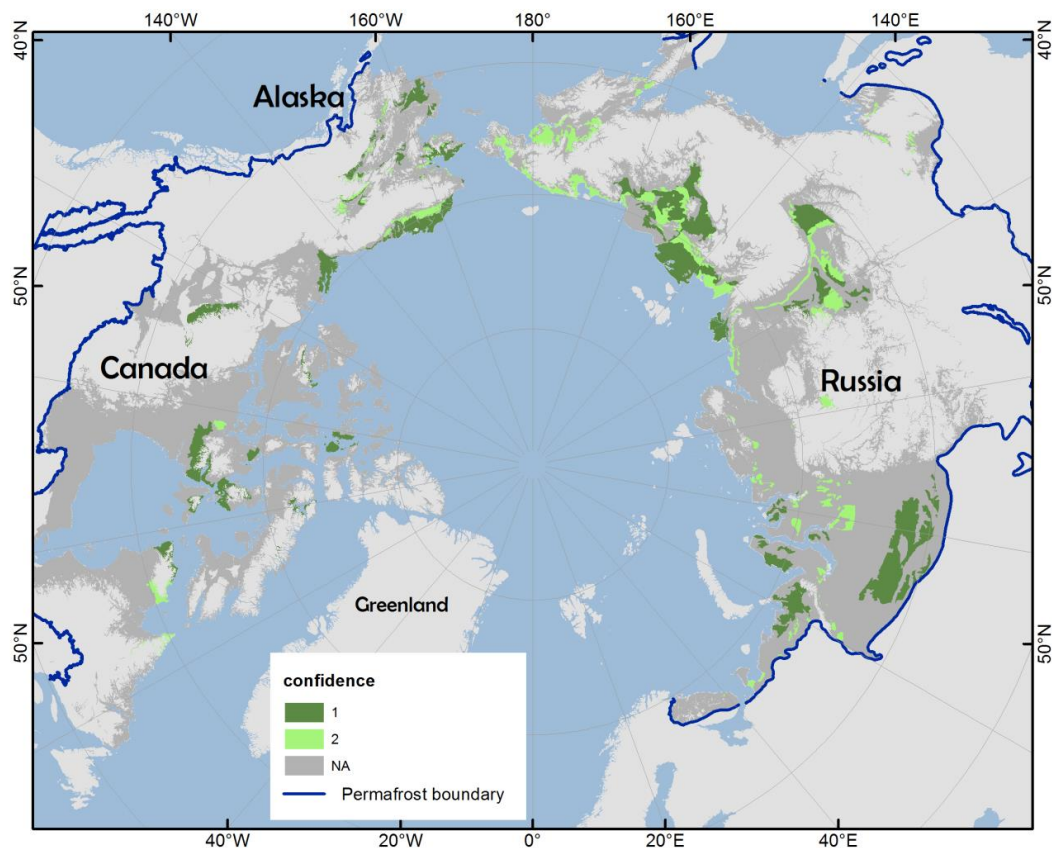
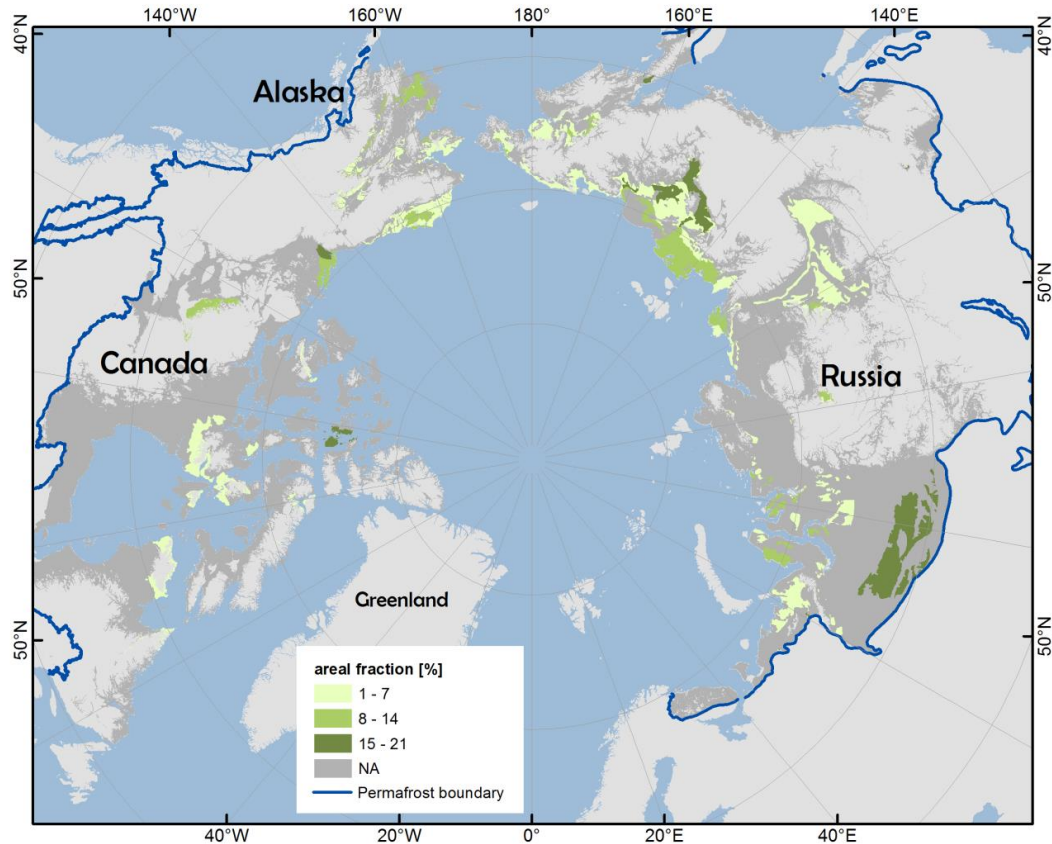
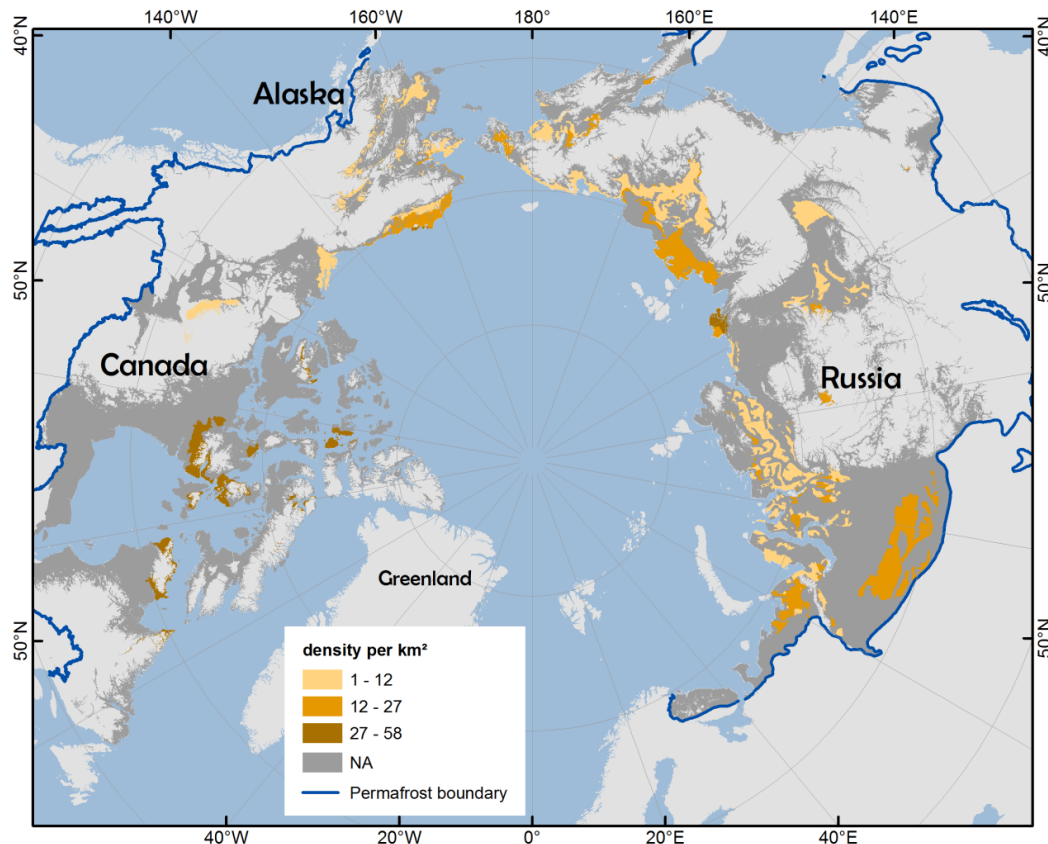


Fig 3: Confidence for permafrost lowland landscapes . Confidence class 1 (high confidence) designates permafrost landscapes where waterbody maps are available in lowland areas. Confidence class 2 (low confidence) represents permafrost landscapes with extrapolated waterbody statistics. No value (dark grey) areas indicate that no maps were available in these permafrost landscapes. Light grey areas indicate terrain with elevations (GTOPO 30, USGS) higher than 300 m a.s.l. which were not considered in the extrapolation. Permafrost boundary was derived from the regional databases.

10



**Figure 4:** Areal fraction of waterbodies with surface areas between  $1.0\text{E}+02 \text{ m}^2$  and  $1.0\text{E}+06 \text{ m}^2$ . Permafrost boundary was derived from the regional databases.



**Figure 5:** Waterbody density per  $\text{km}^2$  for waterbodies with surface areas of between  $1.0\text{E}+02 \text{ m}^2$  and  $1.0\text{E}+06 \text{ m}^2$  within permafrost landscape units. Permafrost boundary was derived from the regional databases.



**Table 3: Extrapolated waterbody statistics for permafrost landscapes. Permafrost extent (PE) is reported as C – continuous, D – discontinuous, S – sporadic, and I – isolated.**  
**Extrapolated statistics include areal fraction and density (frequency per km<sup>2</sup>) for waterbodies (>=1.0E+02 and <=1.0E+02 and >=1.0E+04 m<sup>2</sup>) and ponds (>=1.0E+02 and <=1.0E+04 m<sup>2</sup>).**  
**Numbers in brackets denote the relative error in %.**

country	ecozone	PE	ground ice [vol %]	surficial geology	lithology	fraction	density	pond fraction	pond density
	Arctic Tundra	C	10-40	alluvial-marine	Sandy	7.3 (4.6)	17.6 (3.4)	1.6 (2.8)	16.9 (3.4)
	Arctic Tundra	C	<10	elolian, sand	Sandy	11.1 (4.9)	21.3 (10.3)	1.8 (11.4)	20.4 (10.4)
	Arctic Tundra	C	>40	glaciomarine	Silty	8 (NA)	28 (NA)	1.8 (NA)	27.3 (NA)
Alaska	Bering Taiga	D	>40	elolian, loess	Silty	10.5 (NA)	7.3 (NA)	1.1 (NA)	5.9 (NA)
	Bering Taiga	S	10-40	fluvial, abandoned terrace	Silty	9.9 (5.3)	6.2 (3.8)	0.7 (3.3)	5.1 (3.9)
	Bering Tundra	C	>40	elolian, loess	Silty	5.7 (11.8)	1.6 (18)	0.3 (13.7)	1.1 (28.5)
	Intermontane Boreal	D	10-40	fluvial, abandoned terrace	Silty	7.1 (NA)	2.9 (NA)	0.3 (NA)	2.4 (NA)
	Northern Arctic	C	<20	colluvial fines	Sandy Loam	15.1 (NA)	42.9 (NA)	5.9 (NA)	40.6 (NA)
	Northern Arctic	C	<10	till veneer	NA	3.7 (NA)	57 (NA)	2.1 (NA)	56.7 (NA)
	Southern Arctic	C	>20	glaciofluvial plain	Organic	7.6 (4.5)	5.7 (3.4)	0.5 (3)	5.3 (3.4)
	Southern Arctic	C	>20	till blanket	Clay	13.2 (3.8)	1.9 (3.2)	0.2 (5.3)	1.0 (5.0)
Canada	Southern Arctic	D	>20	alluvial deposits	Loam	7.7 (6.2)	6.9 (5.3)	0.8 (5.2)	6.2 (5.4)
	Taiga Plain	D	>20	alluvial deposits	Loam	21.1 (1.4)	7.6 (1.7)	1.1 (1.8)	5.4 (2.4)
	Taiga Shield	D	<20	till veneer	Sand	8 (13.9)	7.0 (1.9)	1.0 (1.7)	5.8 (1.2)
	Taiga Shield	D	<20	undivided	Sand	10.8 (3.0)	2.7 (2.1)	0.3 (3.4)	1.7 (3.0)
	East Siberian Taiga	C	>40	alluvial-limnetic	Coarse	5.3 (10.1)	1 (8.8)	0 (11.5)	0.7 (9.6)
	East Siberian Taiga	C	>40	alluvial-limnetic	Medium	4.9 (3.8)	2.5 (4.2)	0.4 (4.7)	2.0 (5.0)
	Northeast Siberian Coastal Tundra	C	>40	alluvial-limnetic	Medium	8.3 (NA)	18.2 (NA)	0.8 (NA)	17.6 (NA)
	Northeast Siberian Taiga	C	>40	alluvial-limnetic	Organic	16.7 (10.2)	3.5 (6.3)	0.4 (5.7)	2.3 (6.4)
	Northeast Siberian Taiga	C	>40	alluvial-limnetic cover, loess like deposits, loess and clays	Coarse	5.3 (10.1)	1 (8.8)	0 (11.5)	0.7 (9.6)
Russia	Northeast Siberian Taiga	C	>40	glacial	Medium	1.1 (NA)	3.3 (NA)	0.2 (NA)	3.1 (NA)
	Northwest Russian-Nov.Zem. Tundra	C	<20	alluvial-limnetic	Medium	6.3 (28.1)	12.7 (21.4)	1.4 (24.6)	11.5 (21.5)
	Taimyr-Central Siberian Tundra	C	>40	alluvial-limnetic	Organic	10.3 (10.5)	38.8 (50.1)	2.1 (27.5)	37.8 (51.3)
	Taimyr-Central Siberian Tundra	C	20-40	alluvial-limnetic	Organic	7.2 (NA)	23.8 (NA)	2.5 (NA)	23.1 (NA)
	Taimyr-Central Siberian Tundra	C	20-40	glacial	Medium	3.6 (NA)	4.5 (NA)	0.4 (NA)	4.1 (NA)
	West Siberian Taiga	S	20-40	organic deposits	Organic	16.7 (2.2)	20.2 (2.1)	3 (2.4)	17.6 (2.2)
	Yamal-Gydan Tundra	C	>40	marine	Medium	8.9 (5.0)	3.6 (3.1)	0.4 (2.9)	2.7 (3.2)
	Yamal-Gydan Tundra	C	20-40	marine	Banded	6.1 (2.3)	8.6 (2.7)	0.8 (2.7)	7.8 (2.7)



## 6 Discussion

### 6.1 Classification accuracy and uncertainty

The accuracy of the individual waterbody maps depends on the spectral and spatial properties of the remote sensing imagery employed for classification as well as the classification method. Generally, open water surfaces show a high contrast to the

- 5 surrounding land area in all utilized spectral bands, *i.e.*, panchromatic, near-infrared, and X-band, since water absorbs most of the incoming radiation (Grosse et al., 2005; Muster et al., 2013). Ground surveys of waterbody surface area were available for only a few study sites. Accuracy ranged between 89 % for object-oriented mapping of multispectral (Lara et al., 2015), 93 % for object-oriented mapping of panchromatic imagery (Andresen and Lougheed, 2015), and more than 95 % for a supervised maximum likelihood classification of multispectral aerial images (Muster et al., 2012).
- 10 Different map products were compared for a common area of the Barrow Peninsula. Waterbody areal fraction was 10 % for a Quickbird derived dataset from on August 1, 2002, 6 % for a Komsat dataset from August 2, 2009, and 8 % for a TerraSAR-X dataset from August 25, 2009. The multispectral classification used on the Quickbird image also identifies waterbodies with aquatic vegetation with an areal fraction of 3 %. Many shallow ponds and pond/lake margins are characterized by vegetation growing or floating in the water which cannot be adequately classified from single-band
- 15 imagery (Sannel and Brown, 2010) which is the case for many PeRL classifications. PeRL classifications dating from early August are likely most affected since abundance of aquatic plants peaks around that time of year. In some cases, even multispectral imagery cannot distinguish between lake and land as floating vegetation mats fully underlain by lake water may spectrally appear like a land surface (Parsekian et al. 2011).

### 6.2 Uncertainty of circum-arctic map

- 20 Uncertainties regarding the upscaling of waterbody distributions arise from (i) the combination of different waterbody maps, (ii) the accuracy of the underlying regional permafrost maps, and (iii) the level of generalization inherent in the PL units.

PeRL is a static database that presents late summer inundation conditions only. The effect of image acquisition in relation to rainfall may impact the waterbodies at the site level. However, the effect is hard to quantify as other factors such as spectral properties and resolution also impact classifications of different times at the same site. Average size distributions over large regions probably reduce the importance of seasonal variability as site level variability within the thaw period is being traded for the large spatial coverage of waterbodies across permafrost landscapes.

- 25 Permafrost landscapes present a unified circum-arctic categorization to upscale waterbody distributions. Due to the uncertainty and scale of the regional PL maps, however, it cannot be expected that non-overlapping waterbody maps within the same PL have the same size distribution. The regional permafrost landscape maps are themselves extrapolated products where finite point sources of information have been used to describe larger spatial domains. No error or uncertainty measure, however, was reported for the regional maps. In addition, the variables used to describe permafrost landscapes present the dominant classes within the landscape unit. Thus, certain waterbody maps may represent landscape subtypes that are not represented by the reported average characteristic. For example, two permafrost landscapes have been classified in the Lena Delta in Northern Siberia. The southern and eastern part of the delta is characterized by continuous permafrost with ground ice volumes larger than 40 %, alluvial-limnetic deposits and organic substrate. Local studies differentiate this



region further based on geomorphological differences and ground ice content. The Yedoma ice complex in the southern part features much higher ground ice content of up to 80 % and higher elevations than the eastern part which is however not resolved in the Russian PL map. These sub-regional landscape variations are also reflected in the waterbody size distributions which are significantly different for the southern and eastern part of the delta. In the averaged statistics this is indicated by a high relative error of 11 % and 28 % for areal fraction of waterbodies and ponds, respectively, and about 50 % for density estimates. In this case, the PL unit in that area does not adequately reflect the known distribution of ground ice and geomorphology and demonstrates the need to further improve PL maps in the future.

### 6.3 Potential use of database and future development

Waterbody maps and distribution statistics are most accurate at site-level. At this scale, maps can be used as a baseline to detect changes in surface inundation for seasonal, inter-annual and decadal periods. Site-level size distributions can also be used to validate statistical extrapolation methods which have previously been used to extrapolate from coarser databases to fine scales (Downing et al., 2006; Seekell et al., 2010). Validation of these approaches have since questioned the validity of power laws for smaller lakes but have also been limited to waterbodies as small as  $1.0\text{E}+04 \text{ m}^2$ , *i.e.*, 2 orders of magnitude larger than the minimum size in PeRL data sets.

The circum-arctic map provides spatially extrapolated information for larger-scale applications. Coarse-scale global databases such as the Global Lakes and Wetlands database (GLWD) by Lehner and Döll (2004) are used in global Earth System Models to represent the water fraction in model grid cells (Wania et al., 2013). The GLWD renders a reliable inventory of lakes larger  $1 \text{ km}^2$  (Lehner and Döll, 2004). Compared to the GLWD, PeRL inventoried up to 21 % additional waterbody area. Moreover, ponds are the most frequent waterbody type with 45 to 99 %. In light of observed scaling of biogeochemical processes with waterbody surface area (Wik et al., 2016), PeRL results emphasize the need to include waterbodies of  $1.0\text{E}+06 \text{ m}^2$  and smaller in conjunction with their size distributions in physical and biogeochemical models of the high latitude surface. Moreover, the combination of waterbody size distributions with PL properties can motivate further study for process-based predictive simulations both at the site and regional scale. However, users should be aware of the map's uncertainty when using it to upscale landscape properties such as methane or heat fluxes. For this purpose, users should refer to the reported spatial variability, confidence class and extensive metadata.

PeRL PL units represent the least common denominator across the Arctic where PL properties have been strongly generalized. More detailed information about landscape properties was available for the Canadian database and Northern Alaska (Jorgensen et al., 2014) but not for central and southern Alaska or Russia. We suggest that more detailed and accurate classes of ground ice as well as further refinement of physiography within the broad lowland zone will likely explain differences in waterbody distributions between different maps in the same PL. Regionally different methodologies currently prohibit to compare permafrost landscapes between and to extrapolate across regions. The harmonization of landscape properties, delineation of common terrain units and extrapolation methods for the whole Arctic require a coordinated circum-arctic effort.

Our extrapolated area ( $1.4\text{E}+06 \text{ km}^2$ ) represents only 7.0 % of the current estimated Arctic permafrost area (Brown et al., 1998) but about 17 % of the current Arctic permafrost lowland area (below 300 m a.s.l.) where most of the Arctic lakes are located (Lehner and Döll, 2004; Smith et al., 2007; Grosse et al., 2013). With a few exceptions, the reported sites are predominantly located in coastal areas. Especially the lake-rich permafrost lowlands of Canada and Central Siberia are underrepresented, despite their large spatial coverage. Underrepresented landscape types are areas with discontinuous,



isolated or sporadic permafrost, as well as areas in boreal regions. PeRL maps are conservative estimates of surface inundation as most maps capture open water only and do not include ponds smaller than  $1.0E+02\text{ m}^2$  in size. PeRL maps with resolutions of less than 1 m indicate the presence of many waterbodies smaller than the current threshold of  $1.0E+02\text{ m}^2$ . These very small waterbodies as well as water areas with emerged vegetation are highly productive environments that 5 require attention in future mapping efforts.

## 7 Data availability

Waterbody maps, study area boundaries and maps of regional permafrost landscapes including link to detailed metadata are available at <https://doi.pangaea.de/10.1594/PANGAEA.868349>.

## 8 Conclusions

- 10 PeRL maps and statistics provide a great resource for a large suite of applications across the Arctic such as resource and habitat management, hydrological and ecological modeling, pond and lake change detection, and upscaling of biogeochemical processes. PeRL includes waterbodies with surface areas from  $1.0E+06\text{ m}^2$  down to  $1.0E+02\text{ m}^2$  which complements available global databases and increases waterbody size resolution by 2–4 orders of magnitude. Ponds are the dominant waterbody type found in all study areas across the Arctic. This demonstrates the need to include small 15 waterbodies and parameterize size distributions in global land surface models. Furthermore, PeRL presents a baseline that allows future studies to investigate direction and magnitude of past and future Arctic surface inundation. The current compilation of high-resolution surface inundation maps underlines the need to produce more: vast areas in all regions are still unmapped regarding small waterbodies, especially the Canadian lowlands and boreal regions of Russia. Future mapping efforts should therefore focus on both filling gaps and also monitoring inventoried sites. The combination of 20 waterbody statistics and landscape properties has great potential to improve our understanding of environmental drivers of surface inundation in permafrost lowlands. However, permafrost landscape maps need to be improved by increasing the level of detail as well by harmonizing mapping and extrapolation approaches across Arctic regions.



## Appendix A

**Table A1: Metadata and references for climate data and permafrost depth. MAAT – mean annual air temperature, TP – total precipitation.**

map ID	country	MAAT & TP period	climate data source	permafrost thickness source
abi001	Sweden	2006–2011, 1997–2007	MAAT: Johannesson et al. (2013), TP: Abisko Station, www.polar.se/abisko	Akerman and Johansson (2008), Dobinski (2010)
arg001, arg002	Russia	1999–2011	Boike et al. (2013)	Yershov et al. (1991)
bar001, bar002,	Alaska	1981–2010	National Climatic Data Center (2016); Barrow W Post Rogers Airport AK US	Brown et al. (1980)
bar003, bar004	Russia	1984–1994	Rivas-Martinez (2008)	Grosse et al. (2008)
byk001	Canada	N/A		Smith and Burgess (2000)
byl001	Russia	1984–1994	Rivas-Martinez (2008)	Grosse et al. (2008)
che001, che002, eci003	Alaska	1981–2010	National Climatic Data Center (2016); Barrow W Post Rogers Airport, AK, US	Sellmann and Brown (1973)
elc001, elc002, eci003	Canada	1981–2010	Environment Canada (2016), Tuktoyaktuk A	Taylor and Judge (1981)
esk001	Alaska	1981–2010	National Climatic Data Center (2016); Kuparuk AK US	Jorgenson et al. (2008)
fis001	Russia	1999–2011	Boike et al. (2013)	Yershov et al. (1991)
fir001, fir002, fir003	Canada	1971–2000	Bouchard et al. (2014), Environment Canada (2012)	Smith and Burgess (2002)
gpi001	Canada	1971–2000	Sannel and Kulny (2011), Environment Canada	N/A
hbl001	Russia	1971–2000		Yershov et al. (1991)
ice003	Russia	1999–2011	Boike et al. (2013)	N/A
ind001, kyt001	Russia	1961–1990	Chokurdakh WMO station 21946	Yershov et al. (1991)
kol001	Russia	1996–2015	Bukhta Ambarchik meteorostation (WMO ID 25034)	Yershov et al. (1991)
kol002	Russia	1996–2015	Andrushkino meteorostation (WMO ID 25017)	Yershov et al. (1991)
kur001, kur002	Russia	1999–2011	Boike et al. (2013)	Yershov et al. (1991)
log001	Russia	1961–1990	Khatanga WMO station 20891	N/A
mdn001	Canada	1981–2010	Environment Canada (2016), Inuvik A	Burn and Kokelj (2009)
mdw001	Canada	1981–2010	Environment Canada (2016), Inuvik A	Burn and Kokelj (2009)
ole001	Russia	1948–1980	Rivas-Martinez (2008)	Grosse et al. (2008)
pbp001	Canada	1981–2010	Environment Canada (2016), Resolute Cars	Smith and Burgess (2002)



map ID	country	MAAT & TPP period	climate data source	permafrost thickness source
imc001, kcp001, kpc002, kpc003	Alaska	1981–2010	National Climatic Data Center (2016); Kuparuk AK US	N/A
ric001	Canada	1981–2010	Environment Canada (2016); Inuvik A	Burn (2002)
rgg001, rgg002, rog003, rog004, rog005	Russia	1961–1990	Vorkuta, Hugelius et al. (2011)	Rivkin et al. (2008)
sam001	Russia	1999–2011	Boike et al. (2013)	Yershov et al. (1991)
sei001, sei002	Russia	N/A	Sjöberg et al. (2013)	Rivkin et al. (2008)
ksi001	Alaska	1981–2010	National Climatic Data Center (2016); Nome Municipal Airport AK US	Jorgensen et al. (2008)
sun001	Russia	N/A	Krementski et al. (2003)	Krementski et al. (2003)
tbr001, tea001	Canada	1981–2010	Environment Canada (2016), Yellowknife A	N/A
tav001	Sweden	1971–2000	Sannel and Kuhry (2011)	Sannel and Kuhry (2011)
tuk001	Canada	1981–2010	Environment Canada (2016), Tuktoyaktuk A	Taylor and Judge (1981)
yak001	Russia	1930–2010	Fedorov et al. (2014)	Yershov et al. (1991)
yam001, yam002	Russia	2004–2013	Mare-Sale, Leibman et al. (2014)	Yershov et al. (1991)
yf001	Alaska	1981–2010	National Climatic Data Center (2016); Central Number 2 AK US	Walvoord et al. (2012)
yuk001, yuk002	Alaska	1981–2010	National Climatic Data Center (2016); Bethel Airport AK US	N/A



## Appendix B

**Table B1:** Metadata about base imagery, classification accuracy and classification objects, and associated references. Classifications that include partial lakes, rivers or streams are labelled “no” in the “clean” column.

map ID	filenames	base imagery	acquisition date [YYYY-MM-DD]	resolution [m]	accuracy	classes	min size [m <sup>2</sup> ]	Clean	reference
abi0012010xxxxx	abi0012010xxxxx_ortho_nplaea	Orthophoto (Lannmäteriet, 12014/00691); SPOT5; DEM	2010	1.0	>0.71	open water	21	Yes	this paper
arg00120110829	arg00120110829_k2_nplaea	KOMPSAT-2	2011-08-29	4.0	N/A	open water	64	Yes	this paper
arg0022009xxxxx,	arg0022009xxxxx_re_nplaea,	RapidEye	2009-2011	5.0	0.85	in open water	100	No	Bartsch and Seifert (2012)
fir0032009xxxxx,	fir0032009xxxxx_re_nplaea,					comparison to Kompsat II			
ice0032009xxxxx	ice0032009xxxxx_re_nplaea	aerial imagery	1948-08-04	0.7	N/A	open water	16	Yes	Andresen et al. (2015)
bar00119480804	bar00119480804_ai_nplaea	Quickbird	2002-08-02	0.7	N/A	open water	16	Yes	Andresen et al. (2015)
bar00120020802	bar00120020802_qb_nplaea	Quickbird	2008-07-30	0.7	N/A	open water	16	yes	Andresen et al. (2015)
bar00120080730	bar00120080730_qb_nplaea	WorldView-2	2010-08-10	0.5	0.93	open water	16	yes	Andresen et al. (2015)
bar00120100810	bar00120100810_kw2_nplaea	SPOT-5	2006-07-09	2.5	N/A	open water	30	yes	Grosse et al. (2008)
byk00120060709	byk00120060709_spot_nplaea	GeoEye-1	2010-09-02	0.5	N/A	open water	4	yes	this paper
byj00120100902	byj00120100902_geo_nplaea	IKONOS-2	2002-07-09	1.0	N/A	open water	30	yes	Grosse et al. (2008)
che00120020709	che00120020709_ik02_nplaea	ALOS PRISM	2009-07-24	3.0	0.97	open water	36	yes	Widhalm et al. (2014a, 2014b)
che00220090724	che00220090724_alos_nplaea	TerraSAR-X	2009-08-25	2.5	N/A	open water with emerged vegetation	25	yes	this paper
elc00120090825,	elc00120090825_isx_nplaea,								
bar00220090825,	bar00220090825_isx_nplaea	Quickbird	2002-08-01	0.6	0.89 to 0.95	open water	7.8	yes	Lara et al. (2015)
elc00220020801,	elc00220020801_qb_nplaea,								
bar00320020801	bar00320020801_qb_nplaea	KOMPSAT-2	2009-08-02	4.0	N/A	open water	64	yes	Muster et al. (2013)
elc00320090802,	elc00320090802_k2_nplaea,								



map ID	filenames	base imagery	acquisition date [YYYY-MM-DD]	resolution [m]	accuracy	classes	min size [m <sup>2</sup> ]	Clean	reference
bar00420090802	bar00420090802_k2_nplaea	Quickbird	2008-08	0.6	>0.75	open water	1.5	yes	Lara et al. (2015)
elc004200808xx	elc004200808xx_ir_qb_nplaea	TerraSAR-X	2009-07-27	2.5	N/A	open water	36	yes	this paper
esk00120090727	esk00120090727_isx_nplaea	KOMPSAT-2	2009-09-06	4.0	N/A	open water	64	yes	this paper
fir00120090906	fir00120090906_k2_nplaea	KOMPSAT-2	2011-08-29	4.0	N/A	open water	64	yes	this paper
fir00220110711	fir00220110829_k2_nplaea	Airborne Orthorectified Radar Imagery (IF SAR)	2002-07-15	1.3	N/A	open water	100	Yes	Jones et al. (2013)
fsi00120020715	fsi00120020715_ortri_nplaea	aerial imagery	1959-07-07	0.4	N/A	open water	17	yes	Bouchard et al. (2014)
grp00119590707	grp00119590708_ai_nplaea	QuickBird	2006-07-07	0.61	N/A	open water	13	yes	Bouchard et al. (2014)
grp00120060707	grp00120060708_qb_nplaea	aerial imagery	1954-07-01	1.0	N/A	open water	51	yes	Sannel and Brown (2010), Sannel and Kuhry (2011)
hb00119540701	hb00119540701_ai_nplaea	aerial imagery	1974-06-17	1.0	N/A	open water	53	yes	Sannel and Brown (2010), Sannel and Kuhry (2011)
hb00119740617	hb00119740617_ai_nplaea	QuickBird	2006-07-06	0.6	N/A	open water	55	yes	Sannel and Kuhry (2011)
hb00120060706	hb00120060706_qb_nplaea	QuickBird-2	2004-07-25	0.7	N/A	open water	100	yes	this paper
imc00120040725	imc00120040725_qb02_nplaea	WorldView-1	2009-09-07	0.5	N/A	open water	100	yes	this paper
ind00120090907	ind00120090907_wv1_nplaea	CORONA	1965-07-21	5.0	N/A	open water	200	yes	this paper
kol00119650721	kol00119650721_cor_nplaea	Geoeye	2010-08-05	1.0	N/A	open water	4	yes	this paper
kol00219650721	kol00219650721_cor_nplaea	ALOS PRISM	2008-09-26	2.5	RMSE 5.8 m	open water	187	yes	this paper
kur00120080905	kur00120080905_geo_nplaea	ALOS PRISM	2007-07-28	3.0	0.97	open water	36	yes	Widhalm et al. (2014a, 2014b)
kur00220080926	kur00220080926_ap_nplaea	ALOS PRISM	2007-07-28	3.0	0.97	open water	36	yes	Palmitig et al. (2016)
ky00120070728	ky00120070728_ap_nplaea	QuickBird	2011-08-11	2.4	0.90	open water	23	yes	this paper
log00120110811	log00120110811_qp_nplaea	TerraSAR-X	2009-09-21	2.5	N/A	open water	36	yes	this paper
mdw00120090921	mdw00120090921_isx_nplaea	TerraSAR-X	2010-07-16	2.5	N/A	open water	64	yes	this paper
mdn00120100716	mdn00120100716_isx_nplaea								



map ID	filenames	base imagery	acquisition date [YYYY-MM-DD]	resolution [m]	accuracy	classes	min size [m <sup>2</sup> ]	Clean	reference
ole00120060708	ole00120060708_spot_npelaea	SPOT-5	2006-07-08	2.5	N/A	open water	30	yes	Grosse et al. (2008)
phb00120090813	phb00120090813_tsx_npelaea	TerraSAR-X	2009-08-13	2.5	N/A	open water	12	yes	Müller et al. (2013)
kpc001201007xx,	pru001201007xx_ai_npelaea,	digital true color aerial imagery	2010-07-09 and 07-25	N/A	N/A	open water	1	yes	Walker et al. (2014), Raynolds et al. (2014)
kpc001201007xx,	pru002201007xx_ai_npelaea								
kpc001201007xx,	pru003201007xx_ai_npelaea								
ric001201209125	ric001201209125_tsx_npelaea	TerraSAR-X	2012-09-25	2.5	N/A	open water	8	yes	this paper
rog00120070626	rog00120070626_qb_npelaea	QuickBird	2007-06-26	0.6	N/A	open water	30	yes	Sjöberg et al. (2013)
rog00219740726	rog00219740726_ai_npelaea	aerial imagery	1974-07-26	1.0	N/A	open water	28	yes	Sannel and Kuhry (2011)
rog00220070707	rog00220070707_qb_npelaea	QuickBird	2007-07-07	0.6	N/A	open water	28	yes	Sannel and Kuhry (2011)
rog00320070626	rog00320070626_qb_npelaea	QuickBird-2	2007-06-26	2.4	Overall Kappa: 0.68	open water	11	yes	this paper
rog00420070704	rog00420070704_qb_npelaea	QuickBird-2	2007-07-04	2.4	Overall Kappa: 0.83	open water	29	yes	this paper
rog00520070704	rog00520070704_qb_npelaea	QuickBird-2	2007-07-04	2.4	Overall Kappa: 0.83	open water	11.5	yes	this paper
sam001200808xx	sam001200808xx_ai_npelaea	aerial imagery	2008-08	0.3	N/A	open water	1	yes	Müller et al. (2012)
sei00120070706	sei00120070706_qb_npelaea	QuickBird	2007-07-06	0.6	N/A	open water	30	yes	Sjöberg et al. (2013)
sei00220070706	sei00220070706_qb_npelaea	QuickBird-2	2007-07-06	2.4	Overall Kappa: 0.68	open water	11.5	yes	this paper
ksl0012012xxxx	sew0012012xxxx_spot_npelaea	SPOT-5	2009-2010	2.5	N/A	open water	25	yes	this paper
ksl00119620628	sew00119620628_cor_npelaea	Corona KH4	1962-06-28	6.0	N/A	open water	144	yes	this paper
sur00120130802	sur00120130802_tsx_npelaea	TerraSAR-X	2013-08-02	2.0	N/A	open water	16	yes	this paper
tbr00120100901,	tan00120100901_tsx_npelaea,	TerraSAR-X	2010-09-01	2.5	N/A	open water	36	yes	this paper
tea00120100901	tan00220100901_tsx_npelaea								
tav00119630831	tav00119630831_ai_npelaea	aerial imagery	1963-08-31	0.5	N/A	open water	28	yes	Sannel and Kuhry (2011)
tav00119750810	tav00119750810_ai_npelaea	aerial imagery	1975-08-10	0.9	N/A	open water	28	yes	Sannel and Kuhry (2011)
tav00120030702	tav00120030702_ik02_npelaea	IKONOS	2003-07-02	1.0	N/A	open water	28	yes	Sannel and Kuhry (2011)



map ID	filenames	base imagery	acquisition date [YYYY-MM-DD]	resolution [m]	accuracy	classes	min size [m <sup>2</sup> ]	Clean	reference
tuk00120120723	tuk00120120723_tsx_npaea	TerraSAR-X	2012-07-23	2.5	N/A	open water	36	yes	this paper
yak0012009xxxx	yak0012009xxxx_re_npaea	RapidEye	2009-2011	5.0	0.85	open water	75	no	Bartsch and Seifert (2012)
yam00120080824	yam00120080824_tsx_npaea	TerraSAR-X	2008-08-24	2.5	N/A	open water	36	yes	this paper
yam00220100820	yam00220100820_tsx_npaea	TerraSAR-X	2010-08-20	2.5	N/A	open water	100	yes	this paper
yfl0012011xxxx	yfl0012011xxxx_ai_npaea	aerial imagery	2011-06-18–2011-09-05	1.0	N/A	open water	4	yes	this paper
yuk00120090812,	yuk00120090812_tsx_npaea	TerraSAR-X	2009-08-12	2.5	N/A	open water	36	yes	this paper
yuk00220090812									

site ID	software	pre-processing	classification band(s)	spectral range	classification method	post-processing	data repository
abi0012010xxxx	GDAL, SAGA GIS, Orfeo toolbox	1. Image segmentation using red Orthophoto RGB (1m) and DEM slope (2m) 2. minimum object size 130m <sup>2</sup> ; 2. Classification of watermask: SVM classifier using Red band and slope	(1m) +	610–680 nm	segmentation (SVM)	N/A	N/A
arg00120110829	ENVI	4.8, georeferencing	Near-infrared	760–900 nm	density slice	N/A	N/A
arg0022009xxxx, fir0032009xxxx	ArcGIS 12 N/A	georeferencing, histogram matching routine for radiometric normalization, mosaicking	B, G, R, RE, NIR	blue: 440–510 nm, green: 520–590 nm, red: 630–685 nm, RE: 690–730 nm, NIR: 760–850 nm	object-oriented classification	N/A	<a href="http://geo.tuwien.ac.at/permafrost/">http://geo.tuwien.ac.at/permafrost/</a>
bar00119480804	ENVI 4.4	coregistration and orthorectification using an image-to-image correction (RMSE of 1.0 m)	panchromatic	N/A	object-oriented classification	N/A	N/A

**Table B2:** Metadata about classification software, algorithm



site ID	software	pre-processing	classification band(s)	spectral range	classification method	post-processing	data repository
bar00120020802	ENVI 4.4	coregistration and orthorectification using an image-to-image correction (RMSE of 1.0 m)	panchromatic	445–900 nm	object-oriented classification	N/A	
bar00120080730	ENVI 4.4	coregistration and orthorectification using an image-to-image correction (RMSE of 1.0 m)	panchromatic	445–900 nm	object-oriented classification	N/A	
bar00120100810	ENVI 4.4	coregistration and orthorectification using an image-to-image correction (RMSE of 1.0 m)	panchromatic	450–800 nm	object-oriented classification	N/A	
byk00120060709	ArcGIS	georeferenced to topographic maps of scale 1:100,000	panchromatic	480–710 nm	density slice		
byt00120100902	Geomatica ArcGIS 10.2	pan-sharpening, orthorectification	B, G, R, NIR	450–510 510–580 655–690 780–920 nm	nn, unsupervised classification nn,	k-means to remove classification imperfections, removed	spatial filter on raster major rivers, streams, shadows water bodies < 4 m <sup>2</sup> , major rivers, streams, shadows stream water bodies, man made structures, included: lake ice, turbid and shallow water
che00120020709	ArcGIS	orthorectification	panchromatic	760–850 nm	density slice	removed: shadows, stream water bodies, man made structures, included: lake ice, turbid and shallow water	<a href="https://doi.pangaea.de/10.1594/PANGAEA.A834200">https://doi.pangaea.de/10.1594/PANGAEA.A834200</a>
che00220090724	N/A	N/A	panchromatic	520–770 nm	density slice	N/A	
elc00120090825, bar0220090825	ENVI 4.4	gamma filter (11x1 pixel)	X-Band	wavelength 31 GHz	nn, k-means classification	N/A	
elc00220020801, bar0320020801	ArcGIS eCognition 9.1	10.2, principle component analysis on raster bands, pan-sharpening	R, B, G, IR	450–520 560–600 630–690 nm,	nn, object-oriented classification	N/A	
elc00320090802, bar0420090802	ENVI ArcGIS 10	4.8, georeferencing	Near-infrared	760–890 nm 760–900 nm	density slice	partial rivers, streams and clouds removed	<a href="https://doi.pangaea.de/10.1594/PANGAEA.A786073">https://doi.pangaea.de/10.1594/PANGAEA.A786073</a>



site ID	software	pre-processing	classification band(s)	spectral range	classification method	post-processing	data repository
etc004200808xx	ArcGIS eCognition 9.2	10.2, principle component analysis on raster bands, pan-sharpening	R,B,G,IIR	450–520 nm, 560–600 nm, 630–690 nm, 760–890 nm	object-oriented classification	N/A	
esk0012009090727	ENVI ArcGIS 10	4.8, lee filter (3x3 pixel) (11x11 pixel)	X-Band	wavelength frequency 9.6 GHz	k-means classification	river, streams, shadows removed	
fir00120090906	ENVI ArcGIS 10	4.8, georeferencing	Near-infrared	760–900 nm	density slice	river, streams, shadows removed	
fir00220110711	ENVI ArcGIS 10	4.8, georeferencing	Near-infrared	760–900 nm	density slice	river, streams, shadows removed	
fs00120020715	ENVI 4.5 ArcGIS 10.0	N/A Scanning (1814 dpi); georeferencing (RMSE = 1.8m (4.2pix))	panchromatic black and white	135 or 270 MHz N/A	density slice manual	N/A	
erp00119590707	ArcGIS 10.0	geometric correction convolution resampling	(cubic) panchromatic	450–900 nm	manual	N/A	
erp00120060707	ENVI ArcGIS 9	4.5, resampling of pixel resolution to 0.6 m, georeferenced to QuickBird image from 2006 with RMSE of 0.38–1.42	panchromatic	N/A	manual delineation	N/A	
hb00119740617	ENVI ENVI ArcGIS 9	4.5, resampling of pixel resolution to 0.6 m, georeferenced to QuickBird image from 2006 RMSE of 0.38–1.42	panchromatic	N/A	manual delineation	N/A	
hb00120060706	ENVI ENVI ArcGIS 9	4.5, N/A orthorectification	panchromatic	405–1053 nm	manual delineation	N/A	
imc00120040725	ENVI ArcGIS 10.3	5.0, orthorectification	panchromatic	760–850 nm	density slice	river, streams, shadows removed	
ind00120090907	ENVI ArcGIS 10.3	5.0, orthorectification	panchromatic	400–900 nm	density slice, filter 3x3	opening	
kol00119650721, kol00219650721	ENVI ArcGIS 9	georeferencing	panchromatic	N/A	manual delineation	N/A	
kur00120100805	ENVI ArcGIS 10	4.8, pan-sharpening, (RMSE: 0.36m)	Near-infrared	760–900 nm	unsupervised classification	k-means	river, streams, shadows removed
kur00220080926	PCI Geomatica, ArcGIS 9	orthorectification based on own stereo DEM	panchromatic	520–770 nm	manual delineation	N/A	



site ID	software	pre-processing	classification band(s)	spectral range	classification method	post-processing	data repository
ky00120070728	ENVI ArcGIS 10	4.8, N/A	panchromatic	520–770 nm	density slice	N/A	<a href="https://doi.pangaea.de/10.1594/PANGAEA/A834200">https://doi.pangaea.de/10.1594/PANGAEA/A834200</a>
log00120110811	ENVI 5.1	N/A	NIR, R, G, B	485–830 nm	supervised maximum-likelihood classification	N/A	
mdw00120090921	ENVI ArcGIS 10	4.8, lee filter gamma filter (1x1x1 pixel) (3x3 pixel), X-Band	wavelength frequency 9.6 GHz	31 mm,	k-means classification	river, streams, shadows removed	
mdw00120100716	ENVI ArcGIS 10	4.8, lee filter gamma filter (1x1x1 pixel) (3x3 pixel), georeferenced to topographic maps of scale 1:10,000	wavelength frequency 9.6 GHz	31 mm,	density slice, DN: -28.06 to -14.79	river, streams, shadows removed	
ole00120060708	ArcGIS		panchromatic	480–710 nm	density slice	shadows, stream water bodies, man made structures removed, (lake ice, turbid and shallow water included	
pfp001200909813	ENVI ArcGIS 10	4.8, gamma filter (1x1x1 pixel)	X-Band	wavelength frequency 9.6 GHz	31 mm, density slice	majority filter (7x7 pixel) to reduce spurious pixels in classification	<a href="http://geobotanical.portal.gina.alaska.edu/catalogs/10609-prudhoe-bay-cumulative-impact-map-araynolds-2014">http://geobotanical.portal.gina.alaska.edu/catalogs/10609-prudhoe-bay-cumulative-impact-map-araynolds-2014</a>
kpe001201007xx, kpe002201007xx, kpe003201007xx	N/A	N/A	R, G, B	N/A	manual delineation	N/A	
ric001201209125	ENVI ArcGIS 10	4.8, lee filter gamma filter (1x1x1 pixel)	X-Band	wavelength frequency 9.6 GHz	31 mm, k-means classification	river, streams, shadows removed	
rog00120070626	ArcGIS	N/A	panchromatic	450–900 nm	manual delineation	N/A	
rog00219740726	ENVI ArcGIS 9	4.5, resampling of pixel resolution to 0.6 m, georeferenced to QuickBird image from 2007 with RMSE of 0.20–1.25, aerial photographs, georeferenced to QuickBird image from 2007 (RMSE of 0.17–1.07)	panchromatic	405–1053 nm	manual delineation	N/A	
rog00220070707	ENVI ArcGIS 9	4.5, 4.7,	panchromatic	405–1053 nm	manual delineation	N/A	



site ID	software	pre-processing	classification band(s)	spectral range	classification method	post-processing	data repository
rog00320070626	Classification Definiens Professional 5.0, post processing	in re-georeferenced measured GPS-points	field B, G, R, Near-IR	blue: 450-520 nm, green: 520-600 nm, red: 630-690 nm, NIR: 760-890 nm	supervised, see more in INFO_Qbird_ classification_ version4.pdf	N/A	
rog00420070704	Classification Definiens Professional 5.0, post processing with ArcGIS	in re-georeferenced measured GPS-points	field B, G, R, Near-IR	blue: 450-520 nm, green: 520-600 nm, red: 630-690 nm, NIR: 760-890 nm	supervised, see more in INFO_Qbird_ classification_ version4.pdf	N/A	
rog00520070704	Classification Definiens Professional 5.0, post processing with ArcGIS	in re-georeferenced measured GPS-points	field B, G, R, Near-IR	blue: 450-520 nm, green: 520-600 nm, red: 630-690 nm, NIR: 760-890 nm	supervised, see more in INFO_Qbird_ classification_ version4.pdf	N/A	
sam001200808xx	ENVI ArcGIS 10	4.8, georeferencing	Near-infrared	N/A	N/A	river, streams, shadows removed	
sei00120070706	ArcGIS	N/A	panchromatic	450-900 nm	manual delineation	N/A	
sei00220070706	Classification Definiens Professional 5.0, post processing with ArcGIS	in re-georeferenced measured GPS-points	field B, G, R, Near-IR, TM (RMSE=10 m)	blue: 450-520 nm, green: 520-600 nm, red: 630-690 nm, NIR: 760-890 nm	supervised, see more in INFO_Qbird_ classification_ version4.pdf	N/A	
ksal0012012xxxx	eCognition 8	Principal Component Analysis on visible and IR bands	G, R, NIR	N/A	object-oriented classification	river, streams, shadows removed	
ksl00119620628	ENVI ArcGIS 10	4.8, georeferencing to Landsat ETM & orthorectification,	panchromatic X-Band gamma filter (10x10m)	N/A	density slice	river, streams, shadows removed	
sur00120130802	ENVI ArcGIS 10	4.8, gamma filter (3x3 pixel), resampling of pixel resolution to 0.6 m, georeference to IKONOS image from 2003	wavelength frequency 9.6 GHz	31 mm, frequency 9.6 GHz	threshold classification	artefacts from streets and airport were removed manually	PoRL database
tbr00120100901, tea00120100901	ENVI ArcGIS 10	4.8, lee filter (3x3 pixel), gamma filter (11x11 pixel)	wavelength frequency 9.6 GHz	31 mm, frequency 9.6 GHz	k-means classification	river, streams, shadows removed	
tav00119630831	ENVI ArcGIS 9	4.5, 4.7, m. georeference to IKONOS image from 2003	panchromatic	N/A	manual delineation	N/A	
tav001197508010	ENVI ArcGIS 9	4.5, 4.7, resampling of pixel resolution to 0.6 m, georeference to IKONOS image from 2003 with RMSE of 0.60-2.38	panchromatic	N/A	manual delineation	N/A	



site ID	software	pre-processing	classification band(s)	spectral range	classification method	post-processing	data repository
tav00120030702	ENVI ENVI ArcGIS 9	4.5, 4.7, m	resampling of pixel resolution to 0.6 patchomatic	760–850 nm	manual delineation	N/A	
tuk00120120723	ENVI ArcGIS 10	4.8, lee gamma filter (7x7 pixel) georeferencing, histogram matching routine for radiometric normalization, mosaicking	filter (3x3 pixel), X-Band B, G, R, RE, NIR	wavelength frequency 9.6 GHz blue: green: red: NIR: 760–890 nm	31 mm, k-means classification 450–520 mm, object-oriented classification 520–600 mm, classification 630–690 mm,	river, streams, shadows removed N/A	<a href="http://geo.tuwien.ac.at/permafrost/">http://geo.tuwien.ac.at/permafrost/</a>
yak0012009xxxx							
yam00120080824	ENVI ArcGIS 10	4.8, lee gamma filter (7x7 pixel) gamma filter (3x3 pixel)	filter (3x3 pixel), X-Band B, G, R	wavelength frequency 9.6 GHz -1.9	31 mm, density slice, DN: -2.7 to -1.9	river, streams, shadows removed N/A	
yam00220100820	ENVI ArcGIS 10 eCognition	4.8, lee gamma filter (11x1 pixel) orthorectification	filter (3x3 pixel), X-Band B, G, R	wavelength frequency 9.6 GHz 450–520 nm, 560–600 mm, 630–690 nm, 760– 890 nm	31 mm, density slice, DN: 0 to 40 river, streams, shadows removed N/A		
yf0012011xxxx	ArcGIS 10.2						
yuk00120090812,	ENVI ArcGIS 10	4.8, lee gamma filter (11x1 pixel)	filter (3x3 pixel), X-Band	wavelength frequency 9.6 GHz	31 mm, k-means classification: 15 classes, 5 iterations	river, streams, shadows removed	
yuk00220090812							



## Appendix C

**Table C1: Description of attributes contained in the polygon attribute table of Alaskan permafrost landscapes (*alaska\_perma\_land.shp*)**

Field name	Description	Source
ECOZONE	ecozone	AK2008
GEN_GEOL	generalized geology	AK2008
LITHOLOGY	texture	AK2008
GROUND_ICE	ground ice content [vol %]	AK2008
PF_EXTENT	permafrost extent	AK2008
PERMA_LAND	combined label of PF_EXTENT / GROUND_ICE/GEN_GEOL/LITHOLOGY	PeRL
ECOZID	ecozone ID	PeRL
PERMID	ID for each polygon in the vector file. The first digit stands for the region (1 – Alaska, 2 – Canada, 3 – Russia), digits 2 – 6 identify the single polygon, and the last three digits identify the ecozone.	PeRL
AREA	area of polygon in square meters	PeRL
PERIMETER	perimeter of polygon in square meters	PeRL

5

**Table C2: Description of attributes contained in the polygon attribute table of Canadian permafrost landscapes (*canada\_perma\_land.shp*).**

field name	description	source
ECOZONE	ecozone	NEF
ECOREGION	ecoregion	NEF
ECODISTRICT	ecodistrict	NEF
GEN_GEOL	dominant fraction of generalized (surficial) geology	NEF
LITHOLOGY	dominant fraction of texture	NEF
GROUND_ICE	dominant fraction of ground ice content in vol%	NEF
PF_EXTENT	dominant fraction of permafrost extent	NEF
PERMA_LAND	combined label of PF_EXTENT / GROUND_ICE/GEN_GEOL/LITHOLOGY	PeRL
ECOZID	ecozone ID	PeRL
PERMID	ID for each polygon in the vector file. The first digit stands for the region (1 – Alaska, 2 – Canada, 3 – Russia), digits 2 – 6 identify the single polygon, and the last three digits identify the ecozone.	PeRL
AREA	area of polygon in square meters	PeRL
PERIMETER	perimeter of polygon in square meters	PeRL

10



**Table C3: Description of attributes contained in the polygon attribute table of Russian permafrost landscapes (*russia\_perma\_land.shp*).**

field name	description	source
ECOZONE	Metadata: <a href="http://maps.tnc.org/files/metadata/TNC_Lands.xml">http://maps.tnc.org/files/metadata/TNC_Lands.xml</a>	Olson et al., 2001  Downloaded at <a href="http://maps.tnc.org/gis_data.html#TerreEcos">http://maps.tnc.org/gis_data.html#TerreEcos</a>
GEN_GEOL	Surficial geology	LRR, Stolbovoi et al. (2002c)
LITHOLOGY	Texture	LRR, Stolbovoi et al. (2002c)
GROUND_ICE	ground ice content in vol%	LRR
PF_EXTENT	permafrost extent	LRR
PERMA_LAND	combined label of PF_EXTENT / GROUND_ICE/GEN_GEOL/LITHOLOGY	LRR
ECOZID	ecozone ID	PeRL
PERMID	ID for each polygon in the vector file. The first digit stands for the region (1 – Alaska, 2 – Canada, 3 – Russia), digits 2 – 6 identify the single polygon, and the last three digits identify the ecozone.	PeRL
AREA	area of polygon in square meters	PeRL
PERIMETER	perimeter of polygon in square meters	PeRL

5

**Table C4: Description of attributes contained in the polygon attribute table of circum-arctic permafrost landscapes (*PeRL\_study\_area.shp*)**

field name	description
country	country
Map_ID	ID of individual waterbody map
site	site name
MAAT	mean annual air temperature [°C]
TP	mean annual total precipitation [mm]
PE_DEPTH	Permafrost depth [m]
lat	latitude coordinate of polygon centroid in decimal degrees (WGS84)
long	longitude coordinate of polygon centroid in decimal degrees (WGS84)
AREA	area of polygon in square metres
AREA_SQKM	area of polygon in square kilometres

10



## Appendix D

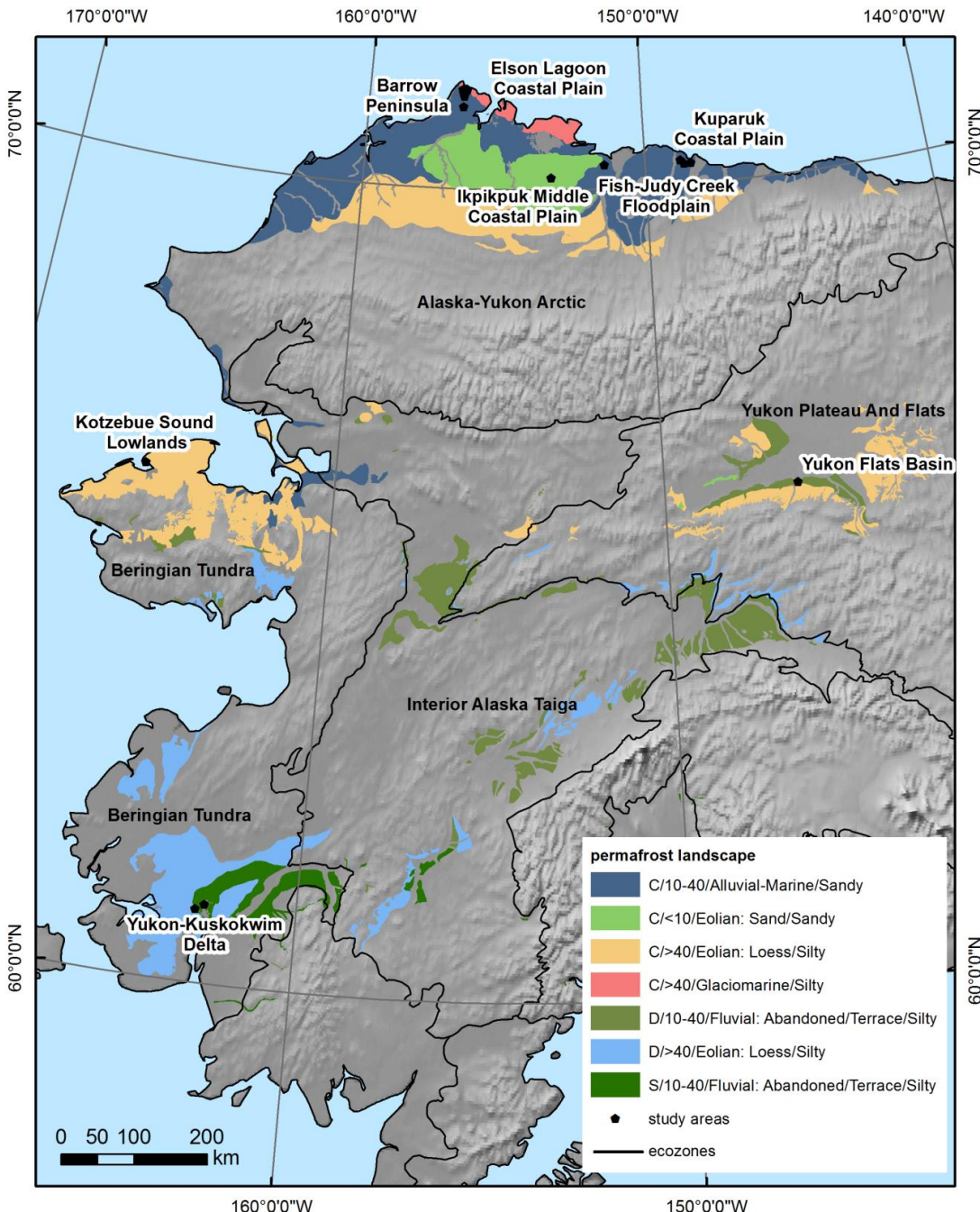
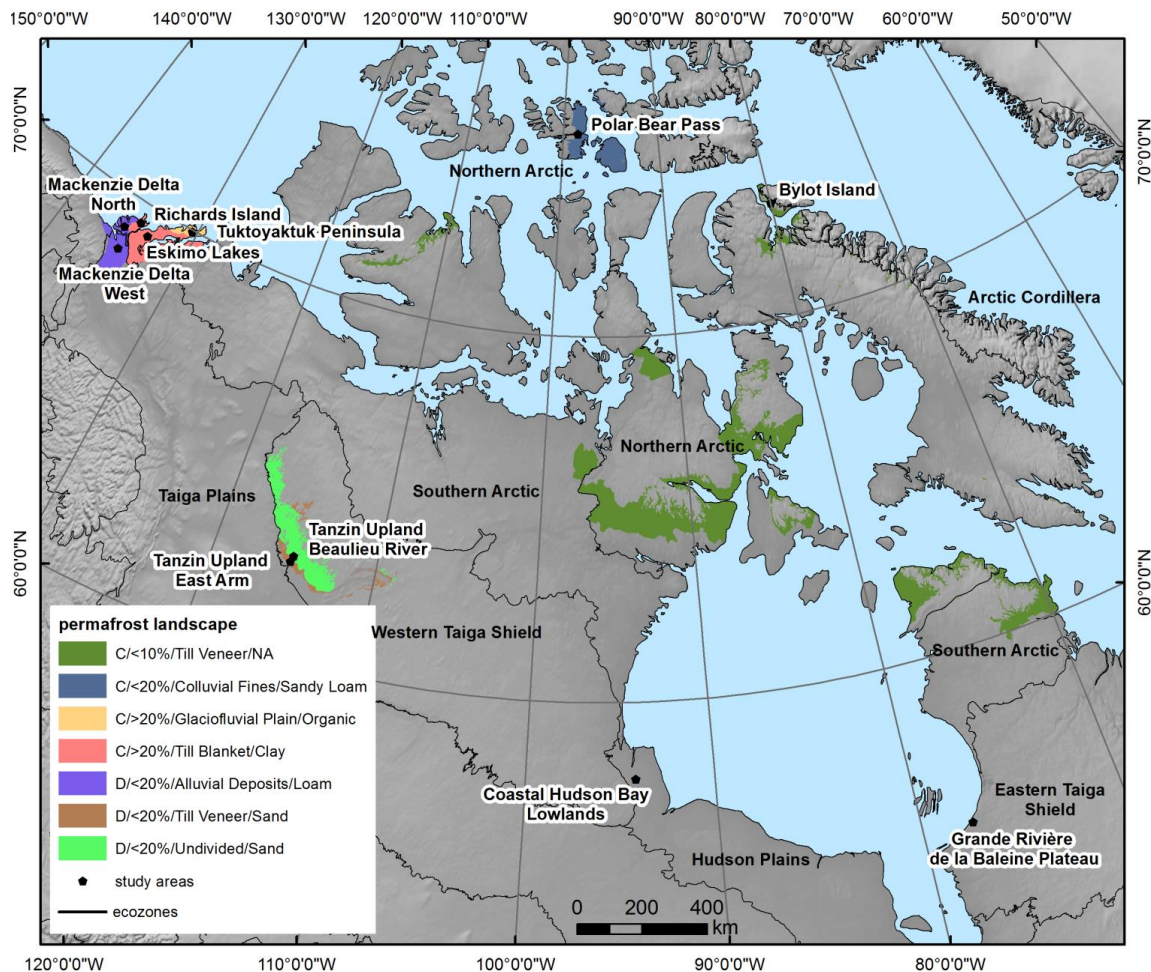


**Figure D1:** Study areas and associated permafrost landscapes in Alaska. Legend lists type of physiography, permafrost extent (C-continuous, D-discontinuous, S-sporadic), ground ice content [vol%], surficial geology and lithology. Shadowed labels name study areas with waterbody maps. Black lines and labels denote ecozones.



5 **Figure D2: Study areas and associated permafrost landscapes in Canada. Legend lists type of physiography, permafrost extent (C-continuous, D-discontinuous, S-sporadic), ground ice content [vol%], surficial geology and lithology. Shadowed labels name study areas with waterbody maps. Black lines and labels denote ecozones.**

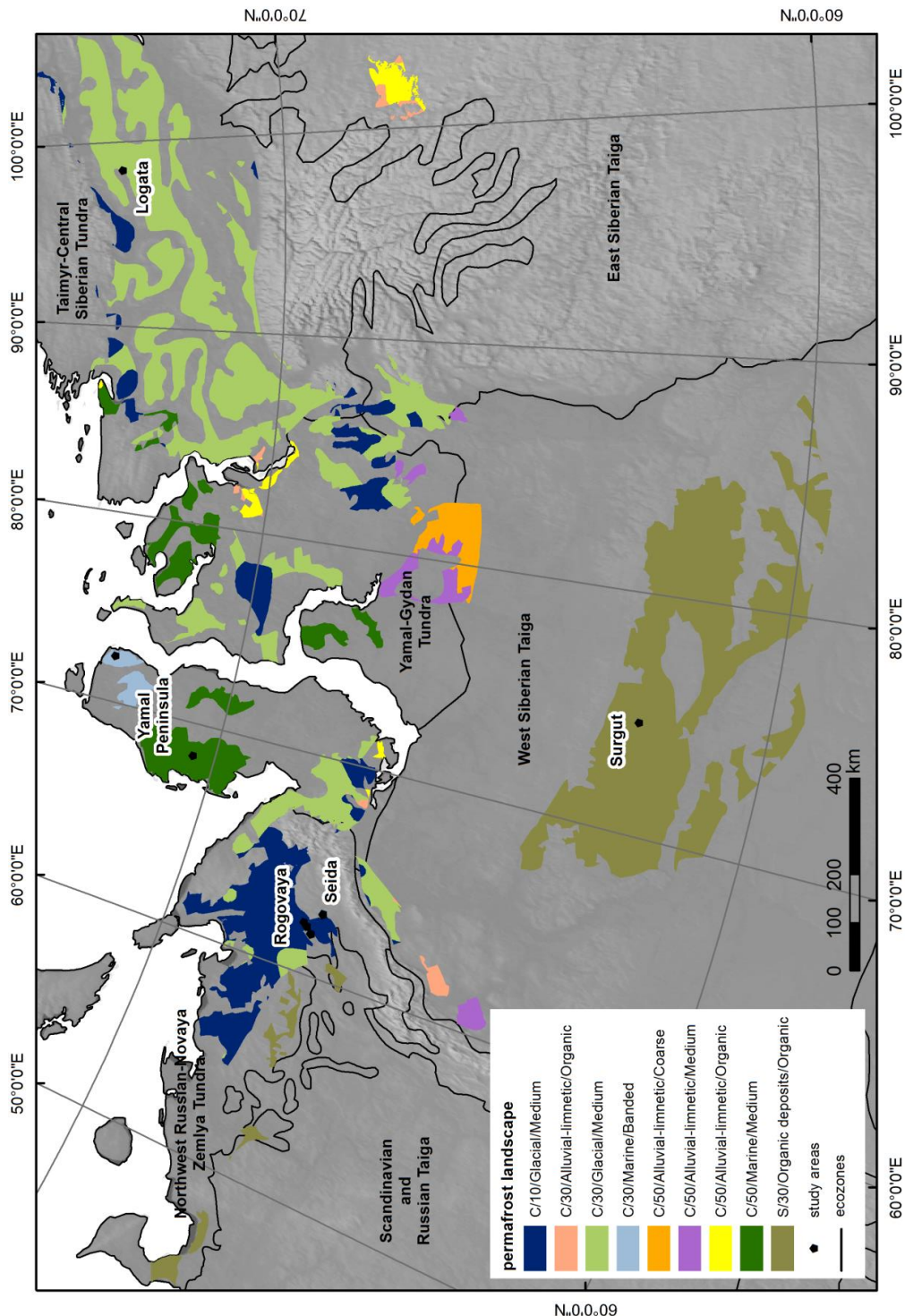


Figure D3: Study areas and associated permafrost landscapes in East Russia. Legend lists type of physiography, permafrost extent (C-continuous, D-discontinuous, S-sporadic), ground ice content [vol%], surficial geology and lithology. Shadowed labels name study areas with waterbody maps. Black lines and labels denote ecozones.

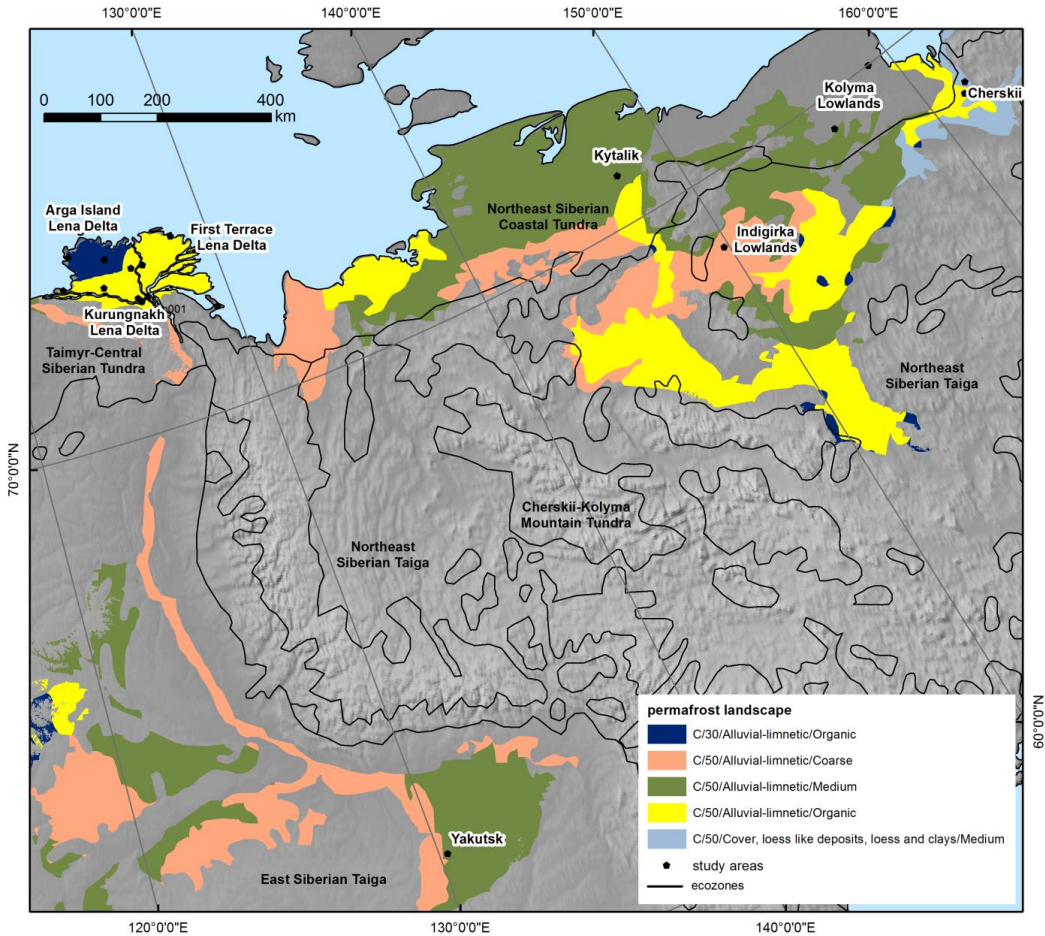


Figure D4: Study areas and associated permafrost landscapes in West Russia. Legend lists type of physiography, permafrost extent (C-continuous, D-discontinuous, S-sporadic), ground ice content [vol%], surficial geology and lithology. Shadowed labels name study areas with waterbody maps. Black lines and labels denote ecozones.



## Appendix E

**Table E1: Areal fraction and density per waterbody map in Alaska. Map IDs with an asterisk were not used for extrapolation. F – areal fraction of waterbodies from 1.0 E+02 m<sup>2</sup> to 1.0 E+06 m<sup>2</sup> in size, REF – relative error of fraction for map subsets of 10x10 km. D – waterbody density per km<sup>2</sup>, RED – relative error of density, PF – pond areal fraction for waterbodies from 1.0 E+02 m<sup>2</sup> to smaller than 1.0 E+04 m<sup>2</sup>, REPF – relative error of pond fraction, PD – pond density, REPD – relative error of pond density.**

map ID	map area	F	REF	D	RED	PF	REPF	PD	REPD
	[km <sup>2</sup> ]	[%]	[%]	[# per km <sup>2</sup> ]	[%]	[%]	[%]	[# per km <sup>2</sup> ]	[%]
bar00119480804	1.9E+01	14	N/A	114	N/A	8	N/A	112	N/A
bar00120020802	1.9E+01	10	N/A	78	N/A	5	N/A	76	N/A
bar00120080730	1.9E+01	11	N/A	78	N/A	6	N/A	76	N/A
bar00120100810	1.9E+01	10	N/A	77	N/A	6	N/A	76	N/A
bar00220090825	1.4E+03	7	5	17	3	2	3	17	3
bar00320020801	1.5E+02	11	N/A	39	N/A	3	N/A	38	N/A
bar00420090802	3.0E+02	6	N/A	13	N/A	1	N/A	12	N/A
elc00120090825	1.3E+02	7	N/A	18	N/A	1	N/A	17	N/A
elc00220020801	1.4E+02	9	N/A	48	N/A	3	N/A	47	N/A
elc00320090802	5.1E+01	7	N/A	18	N/A	1	N/A	17	N/A
fis00120020715	2.4E+02	13	N/A	24	N/A	2	N/A	23	N/A
imc00120040725	1.3E+03	11	5	21	10	2	11	20	10
kcp001201007xx	2.1E+01	22	N/A	49	N/A	7	N/A	46	N/A
kcp002201007xx	2.0E+01	121	N/A	15	N/A	0	N/A	1	N/A
kcp003201007xx	1.9E+01	24	N/A	58	N/A	7	N/A	55	N/A
ksl00119620628	5.6E+02	11	7	12	11	1	10	11	11
ksl0012012xxxx	5.6E+02	6	12	2	18	0	14	1	29
ksl0012012xxxx	5.6E+02	6	12	2	18	0	14	1	29
ycb0012011xxxx	1.0E+02	7	N/A	3	N/A	0	N/A	2	N/A
yuk00120090812	1.1E+03	10	5	6	4	1	3	5	4
yuk00220090812	5.8E+02	10	N/A	7	N/A	1	N/A	6	N/A



**Table E2:** Areal fraction and density per waterbody map in Canada. Map IDs with an asterisk were not used for extrapolation. F – areal fraction of waterbodies from  $1.0 \text{ E+02 m}^2$  to  $1.0 \text{ E+06 m}^2$  in size, REF – relative error of fraction for map subsets of  $10 \times 10 \text{ km}$ . D – waterbody density per  $\text{km}^2$ , RED – relative error of density, PF – pond areal fraction for waterbodies from  $1.0 \text{ E+02 m}^2$  to smaller than  $1.0 \text{ E+04 m}^2$ , REPF – relative error of pond fraction, PD – pond density, REPD – relative error of pond density.

map ID	map area	F	REF	D	RED	PF	REPF	PD	REPD
	[ $\text{km}^2$ ]	[%]	[%]	[# per $\text{km}^2$ ]	[%]	[%]	[%]	[# per $\text{km}^2$ ]	[%]
byl00120100902	4.5E+01	4	N/A	57	N/A	2	N/A	57	N/A
esk00120090727	9.2E+02	14	4	2	3	0	4	1	5
gpr00119590707*	1.8E-01	11	N/A	359	N/A	11	N/A	359	N/A
gpr00120060707*	1.8E-01	11	N/A	326	N/A	11	N/A	326	N/A
hbl00119540701*	4.0E+00	36	N/A	60	N/A	6	N/A	57	N/A
hbl00119740617*	4.0E+00	38	N/A	73	N/A	7	N/A	69	N/A
hbl00120060706*	4.0E+00	35	N/A	60	N/A	6	N/A	56	N/A
mdn00120100716	1.5E+03	8	6	7	5	1	5	6	5
mdw00120090921	1.6E+03	21	1	8	2	1	2	5	2
pbp00120090813	6.9E+01	15	N/A	43	N/A	6	N/A	41	N/A
ric00120120925	5.9E+02	11	8	2	10	0	12	1	11
tbr00120100901	6.9E+02	11	3	3	2	0	3	2	3
tea00120100901	4.6E+02	8	14	7	2	1	2	6	1
tuk00120120723	4.8E+02	8	5	6	3	1	3	5	3

5

**Table E3:** Areal fraction and density per waterbody map in Scandinavia. Map IDs with an asterisk were not used for extrapolation. F – areal fraction of waterbodies from  $1.0 \text{ E+02 m}^2$  to  $1.0 \text{ E+06 m}^2$  in size, REF – relative error of fraction for map subsets of  $10 \times 10 \text{ km}$ . D – waterbody density per  $\text{km}^2$ , RED – relative error of density, PF – pond areal fraction for waterbodies from  $1.0 \text{ E+02 m}^2$  to smaller than  $1.0 \text{ E+04 m}^2$ , REPF – relative error of pond fraction, PD – pond density, REPD – relative error of pond density.

map ID	map area	F	REF	D	RED	PF	REPF	PD	REPD
	[ $\text{km}^2$ ]	[%]	[%]	[# per $\text{km}^2$ ]	[%]	[%]	[%]	[# per $\text{km}^2$ ]	[%]
abi0012010xxxx	3.8E+01	6	N/A	5	N/A	1	N/A	4	N/A
tav00119630831	8.5E-01	15	N/A	40	N/A	4	N/A	34	N/A
tav00119750810	8.5E-01	17	N/A	64	N/A	7	N/A	59	N/A
tav00120030702	8.5E-01	12	N/A	53	N/A	6	N/A	50	N/A



**Table E4: Areal fraction and density per waterbody map in Russia.** Map IDs with an asterisk were not used for extrapolation. F – areal fraction of waterbodies from 1.0 E+02 m<sup>2</sup> to 1.0 E+06 m<sup>2</sup> in size, REF – relative error of fraction for map subsets of 10x10 km. D – waterbody density per km<sup>2</sup>, RED – relative error of density, PF – pond areal fraction for waterbodies from 1.0 E+02 m<sup>2</sup> to smaller than 1.0 E+04 m<sup>2</sup>, REPF – relative error of pond fraction, PD – pond density, REPD – relative error of pond density.

map ID	map area	F	REF	D	RED	PF	REPF	PD	REPD
	[km <sup>2</sup> ]	[%]	[%]	[# per km <sup>2</sup> ]	[%]	[%]	[%]	[# per km <sup>2</sup> ]	[%]
arg00120110829	2.0E+02	7	N/A	24	N/A	2	N/A	23	N/A
arg0022009xxxx*	5.0E+03	9	2	10	2	1	2	9	2
byk00120060709*	1.7E+02	8	N/A	29	N/A	1	N/A	28	N/A
che00120020709	2.2E+02	1	N/A	3	N/A	0	N/A	3	N/A
che00220090724	3.4E+02	17	10	4	6	0	6	2	6
fir00120090906	1.5E+02	9	N/A	36	N/A	2	N/A	35	N/A
fir00220110829	2.2E+02	13	N/A	19	N/A	1	N/A	18	N/A
fir0032009xxxx*	9.8E+03	12	4	21	4	2	4	20	4
ice0032009xxxx*	7.9E+02	1	29	0	22	0	27	0	22
ind00120090907	6.5E+02	5	10	1	9	0	12	1	10
kol00119659721*	2.4E+03	6	4	2	10	0	11	2	12
kol00219659721*	2.6E+03	7	4	1	4	0	4	1	5
kur00120100805*	5.5E+01	8	N/A	14	N/A	1	N/A	13	N/A
kur00220080926	2.5E+02	8	N/A	6	N/A	1	N/A	5	N/A
kyt00120070728	2.6E+02	8	N/A	18	N/A	1	N/A	18	N/A
log00120110811	7.0E+01	4	N/A	5	N/A	0	N/A	4	N/A
ole00120060708	7.5E+01	11	N/A	94	N/A	4	N/A	93	N/A
rog00120070626*	1.0E+01	19	N/A	15	N/A	3	N/A	12	N/A
rog00219740726*	3.4E+00	32	N/A	33	N/A	3	N/A	28	N/A
rog00220070707*	3.4E+00	26	N/A	28	N/A	2	N/A	24	N/A
rog00320070626	6.0E+01	7	N/A	11	N/A	1	N/A	9	N/A
rog00420070704	6.2E+01	10	N/A	11	N/A	2	N/A	9	N/A
rog00520070704	6.3E+01	8	N/A	21	N/A	2	N/A	19	N/A
sam001200808xx*	1.6E+00	14	N/A	116	N/A	5	N/A	114	N/A
sei00120070706*	6.7E+00	8	N/A	49	N/A	4	N/A	48	N/A
sei00220070706	8.3E+01	1	N/A	9	N/A	1	N/A	8	N/A
sur00120130802	1.8E+03	17	2	20	2	3	2	18	2
yak0012009xxxx	2.0E+03	5	4	3	4	0	5	2	5
yam00120080824	1.3E+03	9	5	4	3	0	3	3	3
yam00220100820	1.0E+03	6	2	9	3	1	3	8	3



### Author contributions

S.M. compiled the database, made the analysis and figures, and wrote the manuscript. S.L. assisted in data analysis. All authors contributed to the database compilation and assisted in the writing of the manuscript.

### Acknowledgements

- 5 This work was supported by the Helmholtz Association through a grant (VH-NG 203) awarded to Sina Muster. Any use of trade, product, or firm names is for descriptive purposes only and does not imply endorsement by the US Government. WJR and CDK were supported by the US Department of Energy, BER, under the NGEE-Arctic project under contract no. DE-AC02-05CH11231. Guido Grosse was supported by ERC #338335.
- TerraSAR-X data of Polar Bear Pass, Canada, were acquired through the German Space Agency (DLR) via the project HYD0546. All other TerraSAR -X data in Alaska, Canada, and Russia were made available by DLR via PI agreement LAN1747 within the framework of the ESA funded DUE GlobPermafrost project, FP7 PAGE21 and the Austrian-Russian joint FWF project COLD Yamal (I 1401). RapidEye classifications have been available through the information system of the ESA DUE Permafrost project. Classifications of Rogovaya and Seida sites in Russia were conducted within the CARBONorth project (contract 036993).
- 15 Quickbird-2 and WorldView-1/-2 images (© DigitalGlobe) of Ikpikpuk Middle Coastal Plain, Alaska, and Indigirka Lowlands, Russia, were provided by the Polar Geospatial Center at the University of Minnesota through NSF AON project 1107481. The Geographic Information Network for Alaska (GINA) provided SPOT imagery of the Kotzebue Sound Lowlands, Alaska.

### References

- 20 Abnizova, A., Siemens, J., Langer, M., and Boike, J.: Small ponds with major impact: The relevance of ponds and lakes in permafrost landscapes to carbon dioxide emissions, *Global Biogeochem. Cycles*, 26, 1–9, 2012.
- Andresen, C. G. and Lougheed, V. L.: Disappearing Arctic tundra ponds: Fine-scale analysis of surface hydrology in drained thaw lake basins over a 65 year period (1948–2013), *J. Geophys. Res.-Biogeosci.*, 120, 466–479, 2015.
- Arp, C. D., Whitman, M. S., Jones, B. M., Kemnitz, R., Grosse, G., and Urban, F. E.: Drainage network structure and 25 hydrologic behavior of three lake-rich watersheds on the Arctic Coastal Plain, Alaska, *Arct. Antarct. Alp. Res.*, 44(4), 385–398, 2012.
- Bartsch, A. and Seifert, F. M.: The ESA DUE Permafrost project: A service for high latitude research, 2012 IEEE International Geoscience and Remote Sensing Symposium, Munich, 5222–5225, doi:10.1109/IGARSS.2012.6352432, 2012.
- 30 Barry, T., Berteaux, D., Bültmann, H., Christiansen, J. S., Cook, J. A., Dahlberg, A., ... Ganter, B.: Arctic Biodiversity Assessment 2013. Conservation of Arctic Flora and Fauna (CAFF), 2013.
- Boike, J., Kattenstroth, B., Abramova, K., Bornemann, N., Chetverova, A., Fedorova, I., ... and Hubberten, H.-W.: Baseline characteristics of climate, permafrost, and land cover from a new permafrost observatory in the Lena River Delta, Siberia (1998–2011), *Biogeosciences*, 10, 2105–2128, doi:10.5194/bg-10-2105-2013, 2013.



- Boike, J., Georgi, C., Kirilin, G., Muster, S., Abramova, K., Fedorova, I., Chetverova, A., Grigoriev, M., Bornemann, N., and Langer, M.: Thermal processes of thermokarst lakes in the continuous permafrost zone of northern Siberia – observations and modeling (Lena River Delta, Siberia), *Biogeosciences*, 12, 5941–5965, 2015.
- Boike, J., Grau, T., Heim, B., Günther, F., Langer, M., Muster, S., Gouttevin, I., Lange, S.: Satellite-derived changes in the 5 permafrost landscape of central Yakutia, 2000–2011: Wetting, drying, and fires, *Global Planet. Change*, 139, 116–127, doi:10.1016/j.gloplacha.2016.01.001, 2016.
- Bouchard, F., Francus, P., Pienitz, R., Laurion, I., and Feyte, S.: Subarctic Thermokarst Ponds: Investigating Recent Landscape Evolution and Sediment Dynamics in Thawed Permafrost of Northern Québec (Canada), *Arct. Antarct. Alp. Res.*, 46, 251–271, doi:10.1657/1938-4246-46.1.251, 2014.
- 10 Bouchard, F., Laurion, I., Preskienis, V., Fortier, D., Xu, X., and Whiticar, M. J.: Modern to millennium-old greenhouse gases emitted from ponds and lakes of the Eastern Canadian Arctic (Bylot Island, Nunavut), *Biogeosciences*, 12, 7279–7298, doi:10.5194/bg-12-7279-2015, 2015.
- Brown, J., Ferrians Jr., O. J., Heginbottom, J.A., and Melnikov, E.S.: Circum-arctic map of permafrost and ground ice conditions, National Snow and Ice Data Center, Boulder, CO, USA, 1998, revised February 2001.
- 15 Burn, C. R.: Tundra lakes and permafrost, Richards Island, western Arctic coast, Canada, *Can. J. Earth Sci.*, 39(8), 1281–1298, 2002.
- Burn, C. R. and S. V. Kokelj: The environment and permafrost of the Mackenzie Delta area, *Permafrost Periglac.*, 20(2), 83–105, 2009.
- Carroll, M., Townshend, J., DiMiceli, C., Loboda, T., and Sohlberg, R.: Shrinking lakes of the Arctic: Spatial relationships 20 and trajectory of change, *Geophys. Res. Lett.*, 38, L20406, doi:10.1029/2011GL049427, 2011.
- CAVM Team: Circumpolar Arctic Vegetation Map, Conservation of Arctic Flora and Fauna (CAFF), Map No. 1, 1:7,500,000, U.S. Fish and Wildlife Service, Anchorage, Alaska, USA, 2003.
- Ecological Stratification Working Group: A National Ecological Framework for Canada. Agriculture and Agri-Food Canada, Research Branch, Centre for Land and Biological Resources Research and Environment Canada, State of the 25 Environment Directorate, Ecozone Analysis Branch, Ottawa/Hull. Report and national map at 1:7,500,000 scale, 1995.
- Eineder, M., Fritz, T., Mittermayer, J., Roth, A., Boerner, E., and Breit, H.: TerraSAR-X Ground Segment, Basic Product Specification Document, Technical report, DTIC Document, 2008.
- Environment Canada: Canadian Climate Normals or Averages 1971–2000, [http://climate.weatheroffice.gc.ca/climate\\_normals/index\\_e.html](http://climate.weatheroffice.gc.ca/climate_normals/index_e.html), 2012a.
- 30 Feng, M., Sexton, J. O., Channan, S., and Townshend, J. R.: A global, high-resolution (30 m) inland water body dataset for 2000: first results of a topographic–spectral classification algorithm, *International Journal of Digital Earth*, 9(2), 113–133, 2015.
- Fortier, D., Allard, M., and Shur, Y.: Observation of rapid drainage system development by thermal erosion of ice wedges on Bylot Island, *Canadian Arctic Archipelago, Permafrost Periglac.*, 18, 229–243, 2007.
- 35 Godin, E., Fortier, D., and Coulombe, S.: Effects of thermo-erosion gullying on hydrologic flow networks, discharge and soil loss, *Environ. Res. Lett.*, 9, 105010, doi:10.1088/1748-9326/9/10/105010, 2014.
- Grosse, G., Schirrmeister, L., Kunitsky, V. V., and Hubberten, H. W.: The use of CORONA images in remote sensing of periglacial geomorphology: an illustration from the NE Siberian coast, *Permafrost. Periglac.*, 16(2), 163–172, 2005.



Grosse, G., Romanovsky, V., Walter, K., Morgenstern, A., Lantuit, H., and Zimov, S.: Distribution of thermokarst lakes and ponds at three yedoma sites in Siberia, in: Ninth International Conference on Permafrost, 551–556, 2008.

Grosse, G., Jones, B., and Arp, C.: Thermokarst lakes, drainage, and drained basins, in: Treatise on Geomorphology, Glacial and Periglacial Geomorphology, Academic Press, San Diego, CA, USA, 8, 325–353, 2013.

- 5 Hinzman, L. D., Deal, C. J., McGuire, A. D., Mernild, S. H., Polyakov, I. V., and Walsh, J. E.: Trajectory of the Arctic as an Integrated System, *Ecol. Appl.*, 23, 1837–1868, 2013.

Hugelius, G., Virtanen, T., Kaverin, D., Pastukhov, A., Rivkin, F., Marchenko, S., Romanovsky, V., and Kuhry, P.: High-resolution mapping of ecosystem carbon storage and potential effects of permafrost thaw in periglacial terrain, European Russian Arctic, *J. Geophys. Res.*, 116, G03024, doi:10.1029/2010JG001606, 2011.

- 10 Jershov, E., Kondratjeva, K., Zamolotchkova, S., Trush, N., and Dunajeva, J.: The geocryological map of the USSR, 1:2.500.000, in: Fifth International Conference on Permafrost, 1, 274–277, 1988.

Johansson, M., Callaghan, T. V., Bosiö, J., Åkerman, H. J., Jackowicz-Korczynski, M., and Christensen, T. R.: Rapid responses of permafrost and vegetation to experimentally increased snow cover in sub-arctic Sweden, *Environ. Res. Lett.*, 8(3), 035025, doi:10.1088/1748-9326/8/3/035025, 2013.

- 15 Jones, B. M., Grosse, G. D. A. C., Arp, C. D., Jones, M. C., Walter Anthony, K. M., and Romanovsky, V. E.: Modern thermokarst lake dynamics in the continuous permafrost zone, northern Seward Peninsula, Alaska. *Journal of Geophysical Research: Biogeosciences*, 116(G2), 2011.

Jones, B. M., Gusmeroli, A., Arp, C. D., Strozzi, T., Grosse, G., Gaglioti, B. V., and Whitman, M. S.: Classification of freshwater ice conditions on the Alaskan Arctic Coastal Plain using ground penetrating radar and TerraSAR-X satellite data,

- 20 *Int. J. Remote Sens.*, 34(23), 8267–8279, doi:10.1080/2150704X.2013.834392, 2013.

Jorgenson, M. T., Kanevskiy, M., Shur, Y., Grunblatt, J., Ping, C. L., & Michaelson, G.: Permafrost database development, characterization, and mapping for northern Alaska. Report for Arctic Landscape Conservation Cooperative by Alaska Ecosystem and University of Alaska Fairbanks, 2014.

- 25 Jorgenson, M. T., Yoshikawa, K., Kanevskiy, M., Shur, Y., Romanovsky, V., Marchenko, S., ... and Jones, B.: Permafrost characteristics of Alaska, in: Proceedings of the 9th International Conference on Permafrost, University of Alaska: Fairbanks, 29, 121–122, 2008.

Klonus, S., and Ehlers, M.: Pansharpening with TerraSAR-X and optical data, in: Proceedings of the 3rd TerraSAR-X Science Team Meeting. Darmstadt, Germany: German Aerospace Center (pp. 25-26), 2008.

- Kravtsova, V. I. and Rodionova, T. V.: Variations in size and number of thermokarst lakes in different permafrost regions: 30 spaceborne evidence, *Earth's Cryosphere*, 20(1), 75–81, 2016.

Labrecque, S., Lacelle, D., Duguay, C. R., Lauriol, B., and Hawkin, J.: Contemporary (1951–2001) evolution of lakes in the Old Crow Basin, Northern Yukon, Canada: Remote sensing, numerical modeling, and stable isotope analysis, *Arctic*, 225–238, 2009.

- Langer, M., Westermann, S., Walter Anthony, K., Wischnewski, K., and Boike, J.: Frozen ponds: production and storage of 35 methane during the Arctic winter in a lowland tundra landscape in northern Siberia, Lena River delta, *Biogeosciences*, 12, 977–990, 2015.

Lara, M. J., McGuire, A. D., Euskirchen, E. S., Tweedie, C. E., Hinkel, K. M., Skurikhin, A. N., Romanovsky, V. E., Grosse, G., Bolton, W. R., and Genet, H.: Polygonal tundra geomorphological change in response to warming alters future CO<sub>2</sub> and CH<sub>4</sub> flux on the Barrow Peninsula, *Glob. Change Biol.*, 21, 1634–1651, 2015.



Laurion, I., Vincent, W., MacIntyre, S., Retamal, L., Dupont, C., Francus, P., and Pienitz, R.: Variability in greenhouse gas emissions from permafrost thaw ponds, *Limnol. Oceanogr.*, 55, 115–133, 2010.

Lehner, B. and Döll, P.: Development and validation of a global database of lakes, reservoirs and wetlands, *J. Hydrol.*, 296, 1–22, 2004.

- 5 Leibman, M. O., Khomutov, A. V., Gubarkov, A. A., Dvornikov, Y. A., and Mullanurov, D. R.: The research station "Vaskiny Dachi", Central Yamal, West Siberia, Russia – a review of 25 years of permafrost studies, *Fennia-International Journal of Geography*, 193(1), 3–30, 2014.

Liao, A., Chen, L., Chen, J., He, C., Cao, X., Chen, J., Peng, S., Sun, F., and Gong, P.: High-resolution remote sensing mapping of global land water, *Science China Earth Sciences*, 57, 2305–2316, 2014.

- 10 Liljedahl, A. K., Boike, J., Daanen, R. P., Fedorov, A. N., Frost, G. V., Grosse, G., Hinzman, L. D., Iijima, Y., Jorgenson, J. C., Matveyeva, N., Necsoiu, M., Reynolds, M. K., Romanovsky, V. E., Schulla, J., Tape, K. D., Walker, D. A., Wilson, C. J., Yabuki, H., and Zona, D.: Pan-Arctic ice-wedge degradation in warming permafrost and its influence on tundra hydrology, *Nat. Geosci.*, 9, 312–318, 2016.

Natural Resources Canada: Canada - Permafrost, National Atlas of Canada, 5th edition, Map No. MCR 4177, 1:7.500.000,

- 15 Canada Centre for Mapping, Geomatics Canada and Terrain Sciences Division, Geological Survey of Canada, Ottawa, 1995.

Marshall, I., Schut, P., and Ballard, M.: A National Ecological Framework for Canada: Attribute Data, Technical report, Agriculture and AgriFood Canada, Research Branch, Centre for Land and Biological Resources Research, and Environment Canada, State of the Environment Directorate, Ecozone Analysis Branch, Ottawa/Hull, 1999.

- 20 Muster, S., Langer, M., Heim, B., Westermann, S., and Boike, J.: Subpixel heterogeneity of ice-wedge polygonal tundra: a multi-scale analysis of land cover and evapotranspiration in the Lena River Delta, Siberia, *Tellus B*, 64, 17301, doi:10.3402/tellusb.v64i0.17301, 2012.

Muster, S., Heim, B., Abnizova, A., and Boike, J.: Water Body Distributions Across Scales: A Remote Sensing Based Comparison of Three Arctic Tundra Wetlands, *Remote Sensing*. 2013, 5(4), 1498–1523, 2013.

- 25 Nowacki, G., Spencer, P., Fleming, M., Brock, T., and Jorgenson, T.: Ecoregions of Alaska, U.S. Geological Survey, Open-File Report 02-297, 2001.

Olson, D. M., Dinerstein, E., Wikramanayake, E. D., Burgess, N. D., Powell, G. V., Underwood, E. C., D'amico, J. A., Itoua, I., Strand, H. E., Morrison, J. C., Loucks, C. J., Allnutt, T. F., Ricketts, T. H., Kura, Y., Lamoreux, J. F., Wettengel, W. W., Hedao, P., and Kassem, K. R.: Terrestrial Ecoregions of the World: A New Map of Life on Earth A new global map

- 30 of terrestrial ecoregions provides an innovative tool for conserving biodiversity, *BioScience*, 51, 933–938, 2001.

Palmtag, J., Ramage, J., Hugelius, G., Gentsch, N., Lashchinskiy, N., Richter, A., and Kuhry, P.: Controls on the storage of organic carbon in permafrost soil in northern Siberia, *Eur. J. Soil Sci.*, 67, 478–491, doi:10.1111/ejss.12357, 2016.

Paltan, H., Dash, J., and Edwards, M.: A refined mapping of Arctic lakes using Landsat imagery, *Int. J. Remote Sens.*, 36(23), 5970–5982, 2015.

- 35 Parsekian, A. D., Jones, B. M., Jones, M., Grosse, G., Anthony, W., Katey, M., and Slater, L.: Expansion rate and geometry of floating vegetation mats on the margins of thermokarst lakes, northern Seward Peninsula, Alaska, USA. *Earth Surface Processes and Landforms*, 36(14), 1889–1897, 2011.

Ramsar Convention Secretariat: Designating Ramsar sites: Strategic Framework and guidelines for the future development of the List of Wetland for International Importance, Ramsar handbooks for the wise use of wetlands, 4th edition, vol. 17,



Ramsar Convention Secretariat, Gland, Switzerland, 2010.

Rautio, M., Dufresne, F., Laurion, I., Bonilla, S., Vincent, W., and Christoffersen, K.: Shallow freshwater ecosystems of the

circumpolar Arctic, *Ecoscience*, 18, 204–222, 2011.

Raynolds, M. K., Walker, D. A., Ambrosius, K. J., Brown, J., Everett, K. R., Kanevskiy, M., ... and Webber, P. J.:

- 5 Cumulative geoecological effects of 62 years of infrastructure and climate change in ice-rich permafrost landscapes, Prudhoe Bay Oilfield, Alaska, *Glob. Change Biol.*, 20(4), 1211–1224, 2014.

Riordan, B., Verbyla, D., and McGuire, A. D.: Shrinking ponds in subarctic Alaska based on 1950–2002 remotely sensed images, *J. Geophys. Res.-Biogeosci.*, 111(G4), 2006.

Rivas-Martínez, S.: Worldwide Bioclimatic Classification System, Phytosociological Research Center, Spain:

- 10 <http://www.globalbioclimatics.org>, 2008.

Rivkin, F. M., Vlasova, J. V., Popova, A. P., Mazhitova, G., Kuhry, P., Parmuzin, I. S., and Chehina, I. V.: Mesoscale and detailed geocryological mapping as a basis for carbon budget assessment (east European Russian arctic, CARBO-north project), *in: Proc. 9th Int. Conf. Permafrost*, 2, 1493–1498, 2008.

- 15 Sannel, A. B. K. and Brown, I. A.: High-resolution remote sensing identification of thermokarst lake dynamics in a subarctic peat plateau complex, *Can. J. Remote. Sens.*, 36, 26–40, 2010.

Sannel, A.B.K. and Kuhry, P. : Warming-induced destabilization of peat plateau/thermokarst lake complexes, *Journal of Geophysical Research – Biogeosciences* 116, doi:10.1029/2010JG001635, 2011.

- 20 Santoro, M. and Cartus, O.: STSE-BIOMASAR: Validating a novel biomass retrieval algorithm based on hyper-temporal Wide-Swath and Global Monitoring Envisat ASAR datasets, ESA ESRIN contract No. 21892/08/I-EC, Final Report, 2010,
- Schuur, E. A., Bockheim, J., Canadell, J. G., Euskirchen, E., Field, C. B., Goryachkin, S. V., Hagemann, S., Kuhry, P., Lafleur, P. M., Lee, H., Mazhitova, G., Nelson, F. E., Rinke, A., Romanovsky, V. E., Shiklomanov, N., Tarnocai, C., Venevsky, S., Vogel, J. G., and Zimov, S. A.: Vulnerability of permafrost carbon to climate change: implications for the global carbon cycle, *BioScience*, 58(8), 701–714, 2008.

- 25 Sjöberg, Y., Hugelius, G., and Kuhry, P.: Thermokarst lake morphometry and erosion features in two peat plateau areas of northeast European Russia, *Permafrost Periglac.*, 24(1), 75–81, 2013.

Smith, L. C., Sheng, Y., and MacDonald, G. M.: A first pan-Arctic assessment of the influence of glaciation, permafrost, topography and peatlands on northern hemisphere lake distribution, *Permafrost Periglac.*, 18(2), 201–208, 2007.

Smith, L., Sheng, Y., MacDonald, G., and Hinzman, L.: Disappearing Arctic lakes, *Science*, 308, 1429, 2005.

- 30 Smith, S. and Burgess, M. M.: Ground temperature database for Northern Canada, Open file report 3954, Ottawa, Geological Survey of Canada, 2000.

Smith, S. and Burgess, M. M.: A digital database of permafrost thickness in Canada, Geological Survey of Canada, 2002.

Smith, S. L., Romanovsky, V. E., Lewkowicz, A. G., Burn, C. R., Allard, M., Clow, G. D., Yoshikawa, K., and Throop, J.: Thermal state of permafrost in North America: A contribution to the International Polar Year, *Permafrost Periglac.*, 21, 117–135, doi:10.1002/ppp.690, 2010.

- 35 Soil Landscapes of Canada Working Group: Soil landscapes of Canada version 3.2, Agriculture and Agri-Food Canada, 1:1000000, 2010.

Stolbovoi, V. and McCallum, I.: Land resources of Russia, International Institute for Applied Systems Analysis: [http://webarchive.iiasa.ac.at/Research/FOR/russia\\_cd/download.htm](http://webarchive.iiasa.ac.at/Research/FOR/russia_cd/download.htm), 2002.



Taylor, A. E. and Judge, A. S.: Measurement and prediction of permafrost thickness, Arctic Canada, Technical Papers, 51st Annual Meeting, Society of Exploration Geophysicists, 6, 3964–3977, 1981.

van Huissteden, J., Maximov, T. C., and Dolman, A. J.: High methane flux from an Arctic floodplain (Indigirka lowlands, eastern Siberia), *J. Geophys. Res.*, 110, G02002, doi:10.1029/2005JG000010, 2005.

5 Veremeeva, A. A. and Glushkova, N. V.: Relief formation in the regions of the Ice Complex deposit occurrence: remote sensing and GIS-studies in the Kolyma lowland tundra, *Earth's Cryosphere*, 20(1), 14–24, 2016.

Verpoorter, C., Kutser, T., Seekell, D. A., and Tranvik, L. J.: A global inventory of lakes based on high-resolution satellite imagery, *Geophys. Res. Lett.*, 41, 6396–6402, 2014.

Walker, D. A., Webber, P. J., Walker, M. D., Lederer, N. D., Meehan, R. H., Nordstrand, E. A.: Use of geobotanical maps 10 and automated mapping techniques to examine cumulative impacts in the Prudhoe Bay Oilfield, Alaska, *Environ. Conserv.*, 13, 149–160, 1986b.

Walter, K., Edwards, M., Grosse, G., Zimov, S., and Chapin, F. S.: Thermokarst lakes as a source of atmospheric CH<sub>4</sub> during the last deglaciation, *Science*, 318, 633–635, 2007.

15 Watts, J., Kimball, J., Jones, L., Schroeder, R., and McDonald, K.: Satellite Microwave remote sensing of contrasting surface water inundation changes within the Arctic–Boreal Region, *Remote Sens. Environ.*, 127, 223–236, 2012.

Watts, J. D., Kimball, J. S., Bartsch, A., and McDonald, K. C.: Surface water inundation in the boreal-Arctic: potential impacts on regional methane emissions, *Environ. Res. Lett.*, 9, 075001, 2014.

Widhalm, B., Höglström, E., Ressl, C., Trofaier, A. M., Heim, B., Biasi, C., Bartsch, A.: Land surface hydrology from remotely sensed data at PAGE21 sites with links to geotiff images, doi:10.1594/PANGAEA.834200, 2014a.

20 Widhalm, B., Höglström, E., Ressl, C., Trofaier, A. M., Heim, B., Biasi, C., Bartsch, A.: PAGE21 WP5 - Land surface hydrology from remotely sensed data at PAGE21 sites, Department of Geodesy and Geoinformation (GEO), Research Groups Photogrammetry and Remote Sensing, Vienna University of Technology, 15 pp., \_hdl:10013/epic.43886.d001, 2014b.

Wik, M., Varner, R. K., Anthony, K. W., MacIntyre, S., and Bastviken, D.: Climate-sensitive northern lakes and ponds are 25 critical components of methane release, *Nat. Geosci.*, 9, 99–105, 2016.

Yershov, E. D., Kondrat'yeva, K. A., Loginov, V. F., and Sychev, I. K.: Geocryological Map of Russia and Neighbouring Republics, Faculty of Geology, Chair of Geocryology, Lomonosov Moscow State University, 1991. Yoshikawa, K. and Hinzman, L. D.: Shrinking thermokarst ponds and groundwater dynamics in discontinuous permafrost near Council, Alaska, *Permafrost Periglac.*, 14, 151–160, 2003.